THE OHIO STATE UNIVERSITY

RESEARCH FOUNDATION

1314 KINNEAR ROAD COLUMBUS, OHIO 43212

TECHNICAL REPORT NO. 2

THE EFFECT OF TRANSVERSE ION CURRENT ON THE FLOW OF AIR IN A FLAT DUCT

E. Pejack and H. Velkoff
Department of Mechanical Engineering

U.S. ARMY RESEARCH OFFICE - DURHAM
Box CM, Duke Station
Durham, North Carolina

Contract No. DA-31-124-ARO-D-246

Disclaimer

The findings in this report are not to be construed as an official Department of the Army position.

The citation of trade names and names of manufacturers in this report is not to be construed as official endorsement or approval of commercial products or services rendered.

Distribution of this document is unlimited.

DISCLAIMER NOTICE

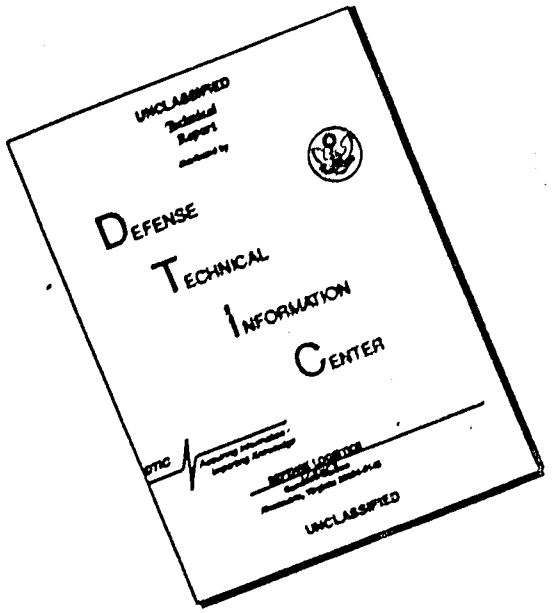

THIS DOCUMENT IS BEST QUALITY AVAILABLE. THE COPY FURNISHED TO DTIC CONTAINED A SIGNIFICANT NUMBER OF PAGES WHICH DO NOT REPRODUCE LEGIBLY.

RF Project 1864

Report No. TR-2

TECHNICAL

REPORT

By

THE OHIO STATE UNIVERSITY
RESEARCH FOUNDATION

1314 KINNEAR RD.
COLUMBUS, OHIO 43212

To U.S. ARMY RESEARCH OFFICE - DURHAM
Box CM, Duke Station
Durham, North Carolina 27706

Contract No. DA-31-124-ARO-D-246

On THE EFFECT OF TRANSVERSE ION CURRENT ON THE FLOW OF AIR IN A FLAT DUCT

Submitted by E. Pejack and H. Velkoff

Department of Mechanical Engineering

Date February, 1967

FOREWORD

This report represents one phase of a general study of the interaction of ions with fluid flows under Contract DA-31-124-ARO-D-246, U. S. Army Research Office - Durham, with Dr. Henry R. Velkoff serving as principal investigator.

The authors wish to thank T. Chuang, K. Diller, D. Smith, I. Anderson, and M. Winiasz for their assistance in various phases of the work reported herein.

ABSTRACT

Friction factors, velocity distributions, pressure gradients, and density measurements were made on a 5/8-inch x 5-inch rectangular flow channel with air flow. A plane of corona wires along the midplane of the channel was the source of ions which drifted across the air flow to the electrically grounded walls of the channel. Experimental data were collected to determine the influence of the ion flow on the air flow and the extent of the ion-fluid coupling.

The electrodynamic and hydrodynamic equations were set up and several approximate solutions were obtained based on the postulation of a flow induced body force and the assumption of fully established, one-dimensional flow. The magnitude of the ion effects was found to be significantly dependent on the ion density distribution within the flow channel.

TABLE OF CONTENTS

LIST OF FIGURES

LIST OF FIGURES (Continued)

LIST OF FIGURES (Continued)

LIST OF SYMBOLS

D	Diffusion coefficient
d_{io}	Collision diameter
E_c	Critical field strength
E_y	Field strength in y direction
E_z	Field strength in z direction
$\vec{F}$	Body force
H	Half height of duct
$\vec{H}$	Magnetic field strength
J_y	Current density in y direction
J_z	Current density in z direction
$\vec{J}$	Current density
k	Boltzmann's constant
K	Mobility
L	Length of duct
m^*	Reduced mass
$N\rho_c$	Charge number
N_1	Charge number
N_2	Charge number
N_3	Charge number
N_{RE}	Reynold's number
n_o	Density of neutral molecules
P	Pressure
P^*	Dimensionless pressure, $P/\frac{1}{2}\rho w_m^2$
R	Gas constant

LIST OF SYMBOLS (Continued)

T	Temperature
u	Velocity component in y direction
$\vec{v}$	Velocity
V	Volts
w	Velocity component in z direction
w_m	Mean velocity
W	Dimensionless velocity, w/w_m
y	Distance coordinate across the flow
z	Distance coordinate along the flow
β	Z/L
ϵ	Permittivity
ξ	Z/L
μ	Viscosity
μ_c	Dielectric permeability
η	Y/H
ρ	Fluid density
ρ_c	Ion density
ρ_{cm}	Mean ion density
σ	Electrical conductivity

SECTION I

INTRODUCTION

The investigation presented in this report is concerned with the flow of slightly ionized air in a rectangualr channel in the presence of an applied electric field. The work presented is an extension of work in which flow of ionized air in a round tube was studied and reported.[1,2,3] The prior work utilized gas flowing along a 1-1/4-inch diameter tube in which a fine wire was located concentrically. A voltage was applied between the wire and the wall of sufficient intensity to produce a corona discharge around the wire and consequently produce unipolar ions in the gas. The results of this prior work indicated large changes in pressure drop, velocity profile, and heat transfer occurred when significnnt ion-currents flowed transverse to the flow. The analysis reported in Reference 3 postulated the existence of an axial body force as a limiting case and the results of the analysis showed order of magnitude agreement with the test data. From the analytical work it could be concluded that the ion-flow coupling mechanism could possibly be active in parallel plate channel flow and in external boundary layers as well. Consequently, studies of the ion-flow coupling effects on boundary layers was extended into parallel-plate channel flow and external flow. This report covers the studies conducted on the parallel plate case, which were aimed at determining whether the trends predicted by the theory for the flat channel would be found to establish the validity of the theory, and above all to secure a better understanding of the basic mechanisms underlying the ion-flow coupling phenomenon.

In the present work, theoretical analyses and experimental tests were carried on using air at atmospheric pressure and temperature with a corona discharge as the source of ionization. Experimental results show that the friction factor of the fluid flowing in the duct is increased by the ion coupling by a factor of approximately two, within the range of tests performed. Approximate solutions have been developed which show similar trends as the experimental results.

SECTION II

APPROXIMATE THEORY

Hydrodynamic Approach

The case of the flow between two infinite parallel flat planes is considered. This model approximates flow in a rectangular channel with a large aspect ratio. Ions of one sign are assumed to be emitted from a midplane and travel across the flow area to the flat plates.

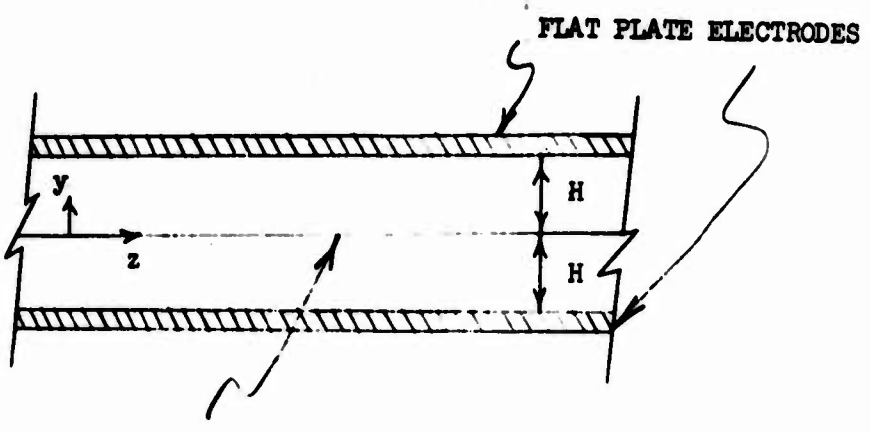

In the hydrodynamic approach, the ions existing in the fluid give rise to a body force per unit volume, $\rho_c E$, acting on the fluid. The following assumptions are also used:

1. The fluid is incompressible.
2. Gravity forces and magnetic forces are negligible.
3. Ionization is produced only on the midplane, and therefore, only ions of one sign exist within the bulk of the fluid.
4. Charge diffusion is negligible.
5. Steady-state conditions exist at all points in the flow field.
6. Non-uniform electric field terms are negligible.
7. Conductivity is small and, therefore, all current is caused by ion motion.
8. The ions have a constant mobility.

The complete set of hydrodynamic and electrodynamic equations for Cartesian coordinates listed in Appendix I then reduce to

$$\rho\left(u\frac{\partial w}{\partial y} + w\frac{\partial w}{\partial z}\right) = -\frac{\partial p}{\partial z} + \mu\left(\frac{\partial^2 w}{\partial y^2} + \frac{\partial^2 w}{\partial z^2}\right) + \rho_c E_z \quad , \tag{1}$$

$$\rho\left(u\frac{\partial u}{\partial y} + w\frac{\partial u}{\partial z}\right) = -\frac{\partial p}{\partial y} + \mu\left(\frac{\partial^2 u}{\partial y^2} + \frac{\partial^2 u}{\partial z^2}\right) + \rho_c E_z \quad , \tag{2}$$

$$\frac{\partial u}{\partial y} + \frac{\partial w}{\partial z} = 0 \quad , \tag{3}$$

$$\rho_c u + \rho_c K E_y = J_y \quad , \tag{4}$$

$$\rho_c w + \rho_c K E_z = J_z \quad , \tag{5}$$

$$\frac{\partial J_y}{\partial y} + \frac{\partial J_z}{\partial z} = 0 \quad , \tag{6}$$

$$\frac{\partial E_y}{\partial z} - \frac{\partial E_z}{\partial y} = 0 \quad , \tag{7}$$

$$\frac{\partial E_z}{\partial z} + \frac{\partial E_y}{\partial y} = \frac{\rho_c}{\epsilon} \quad , \tag{8}$$

Up to this point in the analysis, gradients in the flow direction and fluid motion in the transverse direction are included. The assumption is now made that the velocity and electric fields are "fully established", i.e., all gradients in the z direction except $\partial\rho/\partial z$ are zero and $u = 0$. Then Eq. (6) merely states that J_y is a constant, and J_z appears in Eq. (5) only. The solution of Eq. (1) for the velocity field then requires a specification of J_z.

A limiting solution may be obtained by taking $J_z = 0$. It is seen then that by combining Eq. (5) into Eq. (7) that

$$\frac{1}{K}\frac{\partial w}{\partial y} = 0 \quad , \tag{9}$$

which is satisfied only for $w = 0$ under the assumptions made. (See Appendix II where this difficulty is removed, but then Eq. (8) is not satisfied.) The following solution then will be

a limiting solution for the flow velocity approaching zero, or can be considered as an approximate solution for finite velocity which does not satisfy the irrotational field condition of Eq. (7). Eqs. (1) through (8) become:

$$\frac{\partial p}{\partial z} - \mu \frac{\partial^2 w}{\partial y^2} - \rho_c E_z = 0 \quad , \tag{10}$$

$$\frac{\partial p}{\partial y} - \rho_c E_y = 0 \quad , \tag{11}$$

$$\rho_c K E_y = J_y \quad , \tag{12}$$

$$w + K E_z = 0 \quad , \tag{13}$$

$$\frac{\partial J_y}{\partial y} = 0 \quad , \tag{14}$$

$$\frac{\partial E_z}{\partial y} = 0 \quad , \tag{15}$$

$$\frac{\partial E_y}{\partial y} = \frac{\rho_c}{\epsilon} \quad , \tag{16}$$

From Eq. (14), J_y is a constant. Then substituting ρ_c from Eq. (12) into Eq. (16), it is seen that ρ_c and E_y are uncoupled from the velocity field.

Substituting ρ_c from Eq. (12) into Eq. (16) yields

$$\frac{1}{2} \frac{\partial E_y}{\partial y} = \frac{J_y}{K\epsilon} \tag{17}$$

whose solution is

$$E_y^2 = \frac{2 J_y y}{K\epsilon} + C_1 \tag{18}$$

where C_1 is a constant. This relation has also been developed elsewhere (4).

The boundary condition on E_y specifies the value of the constant C_1. If the ionization is described as "space charge limited", then $E_y = 0$ at $y = 0$ and $C_1 = 0$. Then, the field and ion density profiles are

$$E_y = \left[\frac{2J_y y}{K\epsilon}\right]^{\frac{1}{2}} , \tag{19}$$

and

$$\rho_c = \left[\frac{J_y \epsilon}{2Ky}\right]^{\frac{1}{2}} . \tag{20}$$

The above equation for ρ_c yields an infinite ion density at the midplane, $y = 0$, as a result of the neglect of the ion diffusion term. Ionic diffusion would tend to decrease the ion density near $y = 0$.

According to Eq. (19) the electric field strength is zero at the plane of ionization, $y = 0$, and increases with $y^{1/2}$.

When the ionization plane is a corona discharge, another possible boundary condition is that $E_y = E_c$ at $y = 0$, where E_c is a constant equal to the breakdown field strength of the gas (Ref. 5, p.260). Then $C_1 = E_c^2$ and

$$E_y = \left[\frac{2J_y y + E_c^2 K\epsilon}{K\epsilon}\right]^{\frac{1}{2}} , \tag{21}$$

$$\rho_c = \frac{J_y}{K}\left[\frac{K\epsilon}{2J_y y + E_c^2 K\epsilon}\right]^{\frac{1}{2}} . \tag{22}$$

The solution to the velocity field will be determined first using the field and ion density relation of Eqs. (19) and (20). From Eq. (13), the electric field component in the z direction, E_z, is

$$E_z = -\frac{w}{K} \tag{23}$$

Substituting Eqs. (23) and (20) into Eq. (10) results in the differential equation for the velocity w.

$$u\frac{\partial^2 w}{\partial y} - \frac{1}{K}\sqrt{\frac{J_y \epsilon}{2K}}\, y^{-\frac{1}{2}}\, w - \frac{\partial p}{\partial z} = 0 . \tag{24}$$

The solution of Eq. (24) is listed in Ref. 3 and requires

a numerical evaluation of integrals. An approximate solution can be achieved by replacing $y^{-1/2}$ by its average value over $0 \leq y \leq H$, which is $2H^{-1/2}$. Equation (24) then becomes

$$\mu \frac{\partial^2 w}{\partial y^2} - \frac{1}{K}\left[\frac{2Jy\epsilon}{HK}\right]^{-\frac{1}{2}} w - \frac{\partial p}{\partial z} = 0 \qquad (25)$$

This is equivalent to taking a mean value of the charge density distribution represented by Eq. (19) which yields

$$\rho_{cm} = \left(\frac{Jy\epsilon}{HK}\right)^{\frac{1}{2}} \qquad (26)$$

and then substituting into Eq. (10).

Using H, $\frac{1}{2}\rho w_m^2$, w_m as non-dimensionalizing distance, pressure, and velocity, Eq. (25) in non-dimensional form is

$$\frac{d^2W}{d\eta^2} - N_{\rho c} W - \frac{N_{RE}}{2} \frac{dp^*}{d\xi} = 0 \qquad (27)$$

where W, p^*, η, and ξ are non-dimensional quantities. N_{ρ_c} is called the charge number and is equal to

$$\frac{\rho_{cm} H}{\mu K} = \left[\frac{2Jy_\epsilon}{HK}\right] \frac{H^2}{\mu K} .$$

The Reynolds number N_{RE} is defined as $N_{RE} = \rho \frac{w_m H}{\mu}$.

The hydrodynamic boundary condition is $W = 0$ at $y = \pm H$, the no slip condition at a solid wall, and $\frac{dW}{d\eta} = 0$ at $y = 0$, which means that the ionization plane imparts no shear force to the moving fluid.

The solution to Eq. (27) with the above boundary conditions is

$$W = \frac{-N_{RE}}{2N_{\rho c}} \frac{\partial p^*}{\partial \xi}\left[1 - \frac{\cosh N_{\rho c}^{1/2}\, \eta}{\cosh N_{\rho c}}\right] , \qquad (28)$$

which reduces to the expected parabolic profile

$$W = - N_{RE} \frac{\partial p^*}{\partial \xi}(1-\eta^2) \qquad (29)$$

for $N_{\rho c} \to 0$.

Defining a friction factor $f = -\frac{\partial p^*}{\partial \xi}$ we find from integrating Eq. (28) across the flow area that

$$f = \frac{2\,(2N_{\rho c})^{3/2}}{N_{RE}(N_{\rho c}^{\frac{1}{2}} - \tanh N_{\rho c}^{\frac{1}{2}})} , \tag{30}$$

which reduces to the expected $f = 6/N_{RE}$ for plane Poiseulle flow.

Velkoff [3] also gets an approximate solution to Eq. (24) by taking the second term of that equation equal to a constant, its average value over $0 \le y \le H$. Equation 24 in non-dimensional form is then

$$\frac{\partial^2 W}{\partial y^2} - N_{\rho c} - \frac{N_{RE}}{2}\frac{\partial p^*}{\partial \xi} = 0 . \tag{31}$$

The solution of Eq. (31) with the boundary conditions as before is

$$W = \left[\frac{N_{\rho c}}{2} + \frac{N_{RE}}{4}\frac{\partial p^*}{\partial \xi}\right](\eta^2 - 1) \tag{32}$$

The friction factor $f = -\partial p/\partial \xi$ is

$$f = (1 + \frac{N_{\rho c}}{3}\quad\frac{6}{N_{RE}} \tag{33}$$

which again becomes

$$f = \frac{6}{N_{RE}} \tag{34}$$

for the limiting case of $N_{\rho c} = 0$. Equations (30) and (33) are both approximate solutions of the friction factor derived from Eq. (24). Equation (30) utilized an average value of $y^{-\frac{1}{2}}$ and Eq. (33) utilized an average value of $wy^{-\frac{1}{2}}$ for the solution. They can be regarded then as integral solutions of the friction factor. Figure 1 compares the graphs of the two integral solutions and it is seen that they differ by less than 11% up to a charge number of 4.

The solution to the velocity field will next be determined using the field and ion density profile according to Eqs. (21) and (22). Substituting Eqs. (22) and (23) into Eq. (10) results in the differential equation for the velocity w.

$$\mu \frac{\partial^2 w}{\partial y^2} - \frac{wJ_y}{K^2} \left[\frac{K\epsilon}{2J_y y + E_c^2 K\epsilon} \right]^{1/2} - \frac{\partial p}{\partial z} = 0. \qquad (35)$$

The relative magnitudes of the two terms in the denominator of the second term will be determined. For

$$J_y = 3.33 \times 10^{-6} \text{ amp in.}^{-2}$$

$$y = 0.312 \text{ in. max}$$

$$K = 0.216 \text{ in.}^2 \text{ volt}^{-1}\text{sec}^{-1}$$

$$\epsilon = 2.54 \times 10^{-14} \text{ coul}^2\text{lb}^{-1}\text{in.}^{-2}$$

$$E_c = 76.2 \times 10^3 \text{ volt in.}^{-1} \quad .$$

Then

$$2J_y y = 2.08 \times 10^{-6} \text{ amp in.}^{-1}$$

and

$$E_c^2 K\epsilon = 2.84 \times 10^{-4} \text{ amp in.}^{-1} \quad .$$

Therefore, since $2J_y y$ is negligible compared to $E_c^2 K\epsilon$, it will be neglected. Equation (35) then reduces to

$$\mu \frac{\partial^2 w}{\partial y^2} - \frac{wJ_y}{K^2 E_c} - \frac{\partial p}{\partial z} = 0 \quad . \qquad (36)$$

In nondimensional form

$$\frac{\partial^2 W}{\partial \eta^2} - \left[\frac{J_y H^2}{\mu K^2 E_c} \right] W - \frac{N_{RE}}{2} \frac{\partial p}{\partial \xi} = 0 \quad . \qquad (37)$$

The quantity $J_y H^2/\mu K^2 E_c = N_1$ appears in Eq. (37) in the same position as $N\rho_c$ in Eq. (27). Since

$$\frac{J_y H^2}{\mu K^2 E_c} = \frac{1}{E_c} \left[\frac{J_y H}{2K\epsilon} \right]^{1/2} N\rho_c \quad ,$$

the solution to Eq. (37) is the same as Eq. (28) except that $N\rho_c$ is multiplied by

$$\frac{1}{E_c} \left[\frac{J_y H}{2K\epsilon} \right]^{1/2} .$$

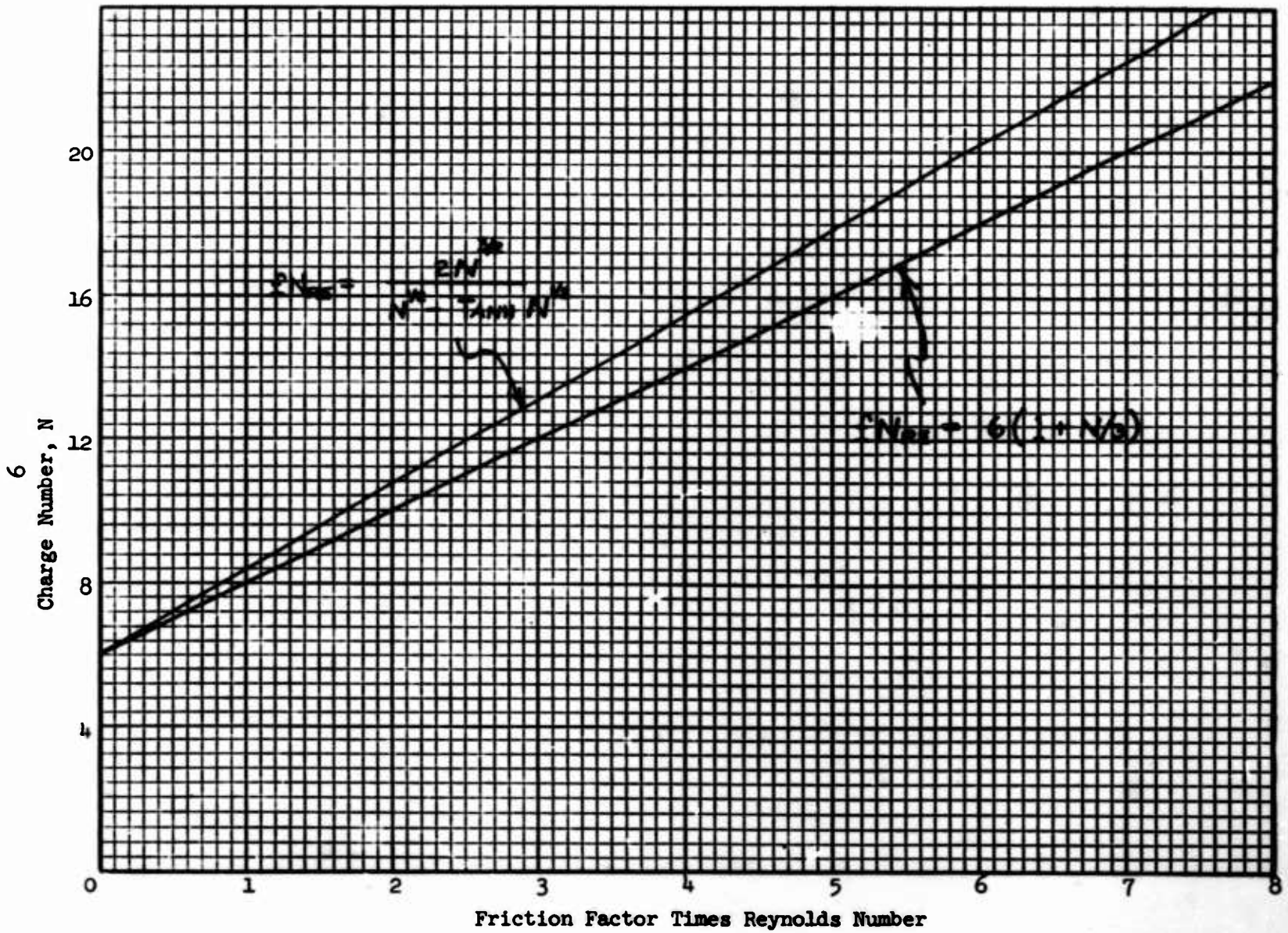

Fig. 1 - Friction factor times Reynolds' number versus charge number for two theoretical models

The solution to Eq. (37) is

$$W = -\frac{N_{RE}}{2N_1}\frac{\partial P}{\partial \xi}\left[1 - \frac{\cosh N_1^{1/2}\eta}{\cosh N_1^{1/2}}\right], \tag{38}$$

and the corresponding friction factor is

$$f = \frac{2N_1^{3/2}}{N_{RE}(N_1^{1/2}-\tanh N_1^{1/2})} . \tag{39}$$

One significant difference between the velocity profile solution using the ion density relation of Eq. (26) and the solution using (22) is that in the former the current density appears in the non-dimensional charge number to the half power, whereas in the latter the current density appears to the first power.

The assumption is sometimes made when dealing with distribution of charges in an electric field that the charges do not affect the electric field. Making this assumption then, the electric field strength is constant,

$$E_y = \frac{V}{H} \tag{40}$$

where V is the voltage applied to the ionization plane, and the walls are at zero potential.

Now from Eq. (12),

$$J_y = \rho_c K E_y$$

$$\rho_c = \frac{J_y}{KE_y} = \frac{J_y H}{KV} \tag{41}$$

Substituting Eqs. (40) and (23) into Eq. (10) results in the differential equation for the velocity field based on no field distortion by ions.

$$\mu\frac{\partial^2 w}{\partial y^2} - \frac{J_y H}{K^2 V} w - \frac{\partial p}{\partial z} = 0 \tag{42}$$

In non-dimensional terms, Eq. (42) becomes

$$\frac{\partial^2 W}{\partial \eta^2} - \frac{J_y H^3}{\mu K^2 V} W - \frac{N_{RE}}{2}\frac{\partial p}{2\xi} = 0 , \tag{43}$$

The non-dimensional parameter $J_yH^3/\mu K^2V = N_2$ appears in Eq. (43) exactly as $N\rho_c$ appears in Eq. (27). The solution therefore, is identical to Eq. (28) with $N\rho_c$ replaced by N_2. Since

$$\frac{J_yH^3}{\mu K^2V} = \frac{1}{V}\left[\frac{J_yH^3}{2K\epsilon}\right]^{1/4} N\rho_c \quad .$$

The non-dimensional parameter in the solution of Eq. (43) is $N\rho_c$ multiplied by

$$\frac{1}{V}\left[\frac{J_yH^3}{2K\epsilon}\right]^{1/4} \quad .$$

The corresponding friction factor is

$$f = \frac{2N_2^{3/2}}{N_{RE}(N_2^{1/4} - \tanh N_2^{1/4})} \quad . \qquad (44)$$

As in Eq. (37), the current density appears in the non-dimensional charge number to the first power.

The approximate theories discussed are tabulated below:

Charge Density Distrubution	Friction Factor	
$\rho_c = \left[\frac{J_yE}{KH}\right]^{1/4}$	$f = \frac{2N\rho_c^{3/2}}{N_{RE}(N\rho_c^{1/4} - \tanh N\rho_c^{1/4})}$	Space charge limited field at midplane, integral solution of Eq. (24) by taking average value of $y^{-1/4}$
	$f = \frac{6}{N_{RE}}\left(1 + \frac{N\rho_c}{3}\right)$	Space charge limited field at midplane, integral solution of Eq. (24) by taking average of $wy^{-1/4}$
$\rho_c = \frac{J_y}{KE_c}$	$f = \frac{2N_1^{3/2}}{N_{RE}(N_1^{1/4} - \tanh N_1^{1/4})}$	Critical field strength at midplane
$\rho_c = \frac{J_yH}{KV}$	$f = \frac{2N_2^{3/2}}{N_{RE}(N_2^{1/4} - \tanh N_2^{1/4})}$	No distortion of field by charges

where

$$N\rho_c = \left[\frac{2J_y \epsilon}{HK} \right]^{1/4} \frac{H^2}{\mu K}$$

$$N_1 = \frac{J_y H^2}{\mu K^2 E_c}$$

$$N_2 = \frac{J_y H^3}{\mu K^2 V} \quad .$$

In the table above there are only two different functional relations between friction factor and charge number, which are shown plotted in Fig. 1.

If $f = \partial p'/\partial \xi$ from Eq. (30) is substituted in Eq. (28), there results the expression for the non-dimensional velocity distribution as a function of charge number.

$$W = \left[1 - \frac{\cosh N\rho_c^{1/4} \eta}{\cosh N\rho_c^{1/4}} \right] \left[1 - \frac{\tanh N\rho_c^{1/4}}{N\rho_c^{1/4}} \right] \tag{45}$$

Figure 2 shows the shape of the velocity distribution from Eq. (45) with charge number as a parameter. The velocity distribution becomes flattened in the central region of the flow channel with increasing charge number, in exact analogy with Hartmann flow in magnetohydrodynamics.

Kinetic Theory Approach

The kinetic theory approach treats the ions as being discrete particles dispersed within a fluid. If the ions have a statistically different motion than the molecules of the main fluid, then forces on the main fluid arise because of collision between the ions and neutral particle.

Considering flow between infinite parallel plates and using the same notation as before, the equation for the velocity is, from Refs. 6 and 7

$$\mu \frac{\partial^2 w}{\partial y^2} = \frac{\partial p}{\partial z} + \frac{8}{3} [2m^* \pi kT]^{1/2} d_{io}^2 n_o \rho_c (w - w_i) \tag{46}$$

where

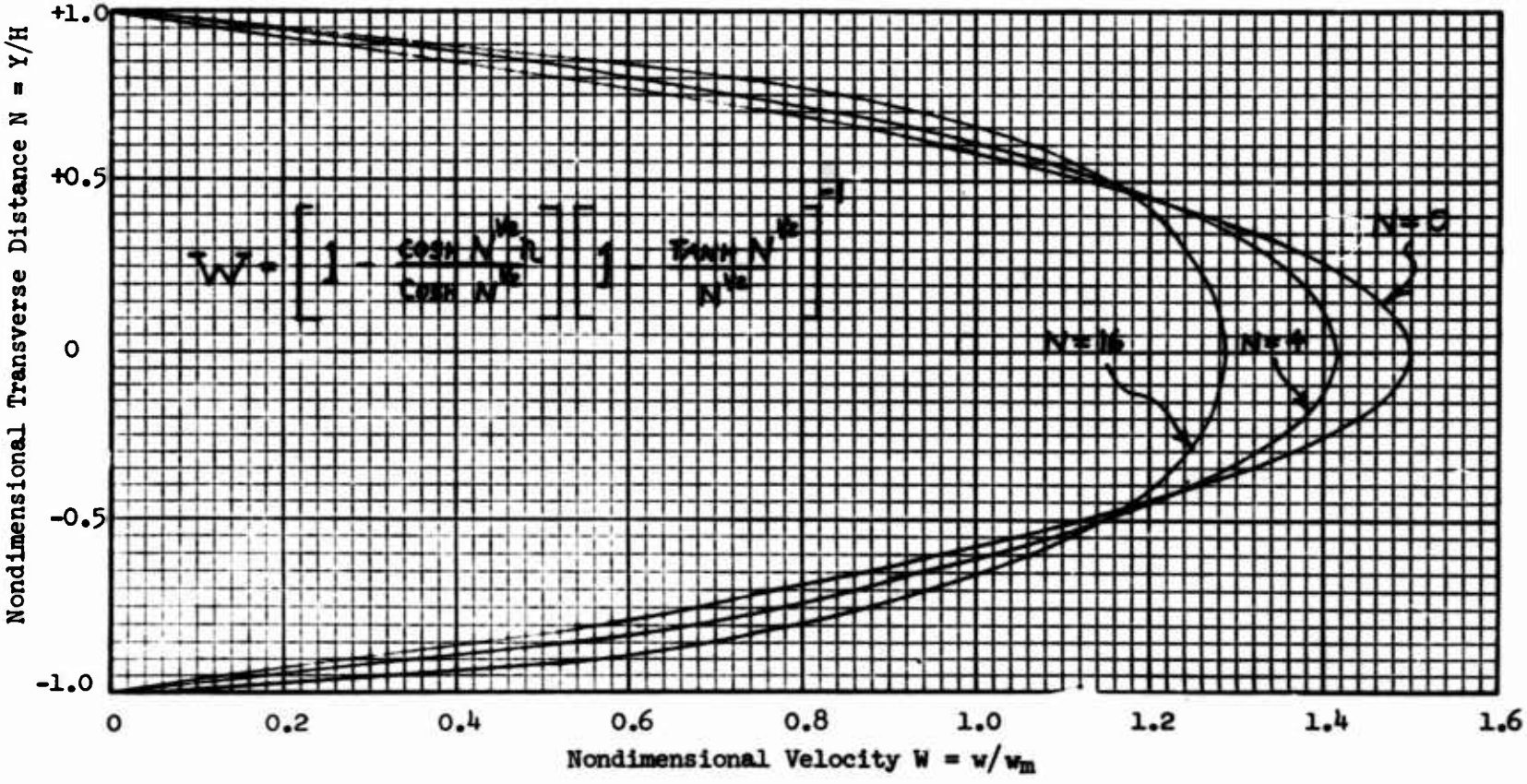

Fig. 2 - Nondimensional velocity profile showing the effect of charge number, based on a theoretical model

m^* = reduced mass $m_i m_o / m_i + m_o$

m_i, m_o = mass of ion and mass of neutral particle

T = absolute temperature

$d_{io} = 1/2\ (d_i + d_o)$

d_i, d_o = diameter of ion and diameter of neutral particle

ρ_c, n_o = number density of ions and neutral particles

w_i = statistical average velocity of ion

The last term in Eq. (46) is analogous to a body force per unit volume in the hydrodynamic formulation. The solution of Eq. (46) requires a specification of w_i, the ion velocity. The greatest contribution of the last term of Eq. (46) occurs for $w_i = 0$, which would mean that the ions travel across the flow with no downstream motion. This is exactly the same simplifying assumption used earlier when J_z was taken equal to zero. The solution to Eq. (46) will be obtained using $w_i = 0$; the friction factor thus obtained will be an upper limit on the effect of ionic coupling to the mean flow.

First nondimensionalizing Eq. (46),

$$\frac{\partial^2 w}{\partial \eta^2} - \frac{8}{3} [2\pi m^* kT]^{1/2} d_{io}^2\, n_o\, \rho_c \frac{H^2}{\mu} W - \frac{N_{RE}}{2} \frac{\partial p}{\partial \xi} = 0 \quad . \tag{47}$$

Comparing Eq. (47) with Eq. (27), the quantity

$$\frac{8}{3} [2\pi m^* kT]^{1/2} d_{io}^2\, n_o\, \rho_c \frac{H^2}{\mu} = N_3 \tag{48}$$

is exactly analogous to $N\rho_c$.

Since ρ_c, the ion number density can possibly be a function of y, the solution of Eq. (47) requires a separate solution of the electrodynamic equations to obtain ρ_c. This requirement is the same as the requirement of obtaining ρ_c in the hydrodynamic formulation.

For the assumption of ρ_c = constant = Jy/KE_c, (which led to nondimensional parameter N_1 in the hydrodynamic formulation) and

$m_i = m_o = 1.02 \times 10^{-25}$ LBM/Molecule

$m^* = 5.13 \times 10^{-26}$ LBM/Molecule

$$d_{io} = d_i = d_o = 1.48 \times 10^{-8} \text{ in.}$$

$$T = 300^\circ K$$

$$n_o = 4.03 \times 10^{20} \text{ Molecules in.}^{-3}$$

$$\mu = 1.23 \times 10^{-5} \text{ lbm ft}^{-1}\text{sec}^{-1}$$

$$H = 0.312 \text{ in.}$$

$$K = 0.216 \text{ in.}^2 \text{ volt}^{-1}\text{sec}^{-1}$$

$$E_c = 76.2 \times 10^3 \text{ volt in.}^{-1}$$

we find

$$N_3 = 0.20\ N_1 \tag{49}$$

and for

$$\rho_c = \left[\frac{J_Y \epsilon}{KH} \right]^{1/4}$$

which led to the nondimensional parameter $N\rho_c$ in the hydrodynamic formulation, we find

$$N_3 = 0.14\ N\rho_c \quad . \tag{50}$$

The kinetic approach leads to the identical problem as the hydrodynamic formulation, i.e., the ion number density ρ_c must be specified for a determination of the parameter equivalent to the charge number. For numerical values of the quantities resulting from the kinetic approach, the resulting nondimensional parameter is seen to be less than the analogous nondimensional parameter resulting from the hydrodynamic approach, based on the same ion density.

The simple kinetic approach assumes that momentum is transferred by collision of ions and neutral particles, treated as hard spheres which exert forces only on collision. Since changed particles can exchange momentum without actually colliding in the narrow sense, close agreement in the determination of the charge number between the simple kinetic approach, and the hydrodynamic approach is not expected.

SECTION III

EXPERIMENTAL

Description of Flow Channels

The production of ions in all phases of the test work was achieved by the positive corona discharge mechanism. A high positive voltage was applied to thin steel wires, with a grounded electrode, usually the duct walls, located nearby. The resulting electric field is much more intense near the wires than near the ground electrode, and if the applied voltage is above a critical value, breakdown of the air in the high field region near the wire results in ionization of the air.

Within the region near the wire where ionization takes place these exist both negative and positive ions; the negative ions or electrons travel to the wire and the positive ions travel out of the ionization region and drift toward the grounded electrode. Except for the thin region near the wire then, the fluid under investigation consists of air containing drifting positive ions.

Since the applied voltage is the cause of the ionization and is also the cause of the positive ion drift, it is clear that the amount of ionization and drift velocity are not independent for this method of ion-flow tests. Variation in drift velocity and ion current could, however, be achieved by using wires of different diameters.

The first rectangular channel to be constructed under the test program was a 1/4 inch 5 t inch x 3 foot long duct with one 5-inch side as the grounded electrode. Wires (0.004-inch dia) were stretched along the opposite 5-inch side in the flow direction. The wires were spaced 1/4-inch apart and located tangent to the wall surface.

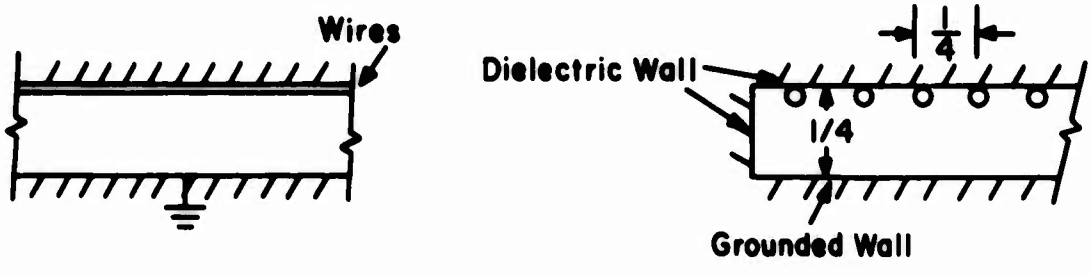

The flow channel with no voltage on the wires would closely approximate flow through a rectangular duct, and serve as a definite limiting case for the study of the ion coupling phenomenon.

With the application of slowly increasing voltages to the wires in the above channel, it was observed that a constant current was not obtainable, but rather frequent arcing and spark discharges occurred. At this time it was postulated that the proximity of the dielectric wall (Plexiglas) was in some way affecting the cornona discharge mechanism. To further investigate this occurrence, some test work was performed to measure the effect of a dielectric surface near a corona wire. This work is described in Appendix III where it is shown that the proximity of a surface to a corona discharge greatly affects the corona characteristics.

Since the main object of the study was the ion flow coupling with air flow, another rectangular duct 5/8 inch x 5 inches x 10 feet long was constructed as shown in Figs. 3-7.

The corona wires were stretched lengthwise along the midplane of the channel, thereby obviating the surface effect noticed in the earlier flow channel.

Static pressure taps were located along the centerline of the upper 5-inch wall at one-foot intervals along the duct length. Traversing total pressure probes, constructed of glass, were located at distances of 5, 9, and 9.8 feet from the duct inlet (hereafter referred to as Positions A, B, and C, respectively). Probes at Positions A and C were located in the center of the duct in the transverse direction and hence traversed the duct cross section midway between two corona wires; the probe at Postion B was directly over a wire and hence, only traversed half the height of the duct.

The output from the high-voltage supply was connected to ten variable resistors in parallel (Fig. 5). Each resistor was in turn connected to one of the ten corona wires in the duct; then with a given voltage setting on the high-voltage supply, the voltage drop across the variable resistors enabled a different voltage to appear on each cornona wire by adjusting the resistor. The voltage adjustment was necessary since each wire has a slightly different ampere-voltage characteristic (Fig 8), and it was desired to maintain equal currents in each wire. For all tests performed, the resistors were so adjusted that a uniform current existed in each wire. From Fig. 8 then it is seen, from the variation in voltage at a given current, that the voltages appearing on the wires could differ from each other by up to 150 volts. The range of voltage applied to the corona wires for all test work on the duct was 5000 to 5700 volts (Fig. 8).

Electrical Characteristics of the Test Apparatus

Upon application of the high voltage to the corona wires, a uniform blue corona glow was observed and repeatable ampere-volt characteristics were

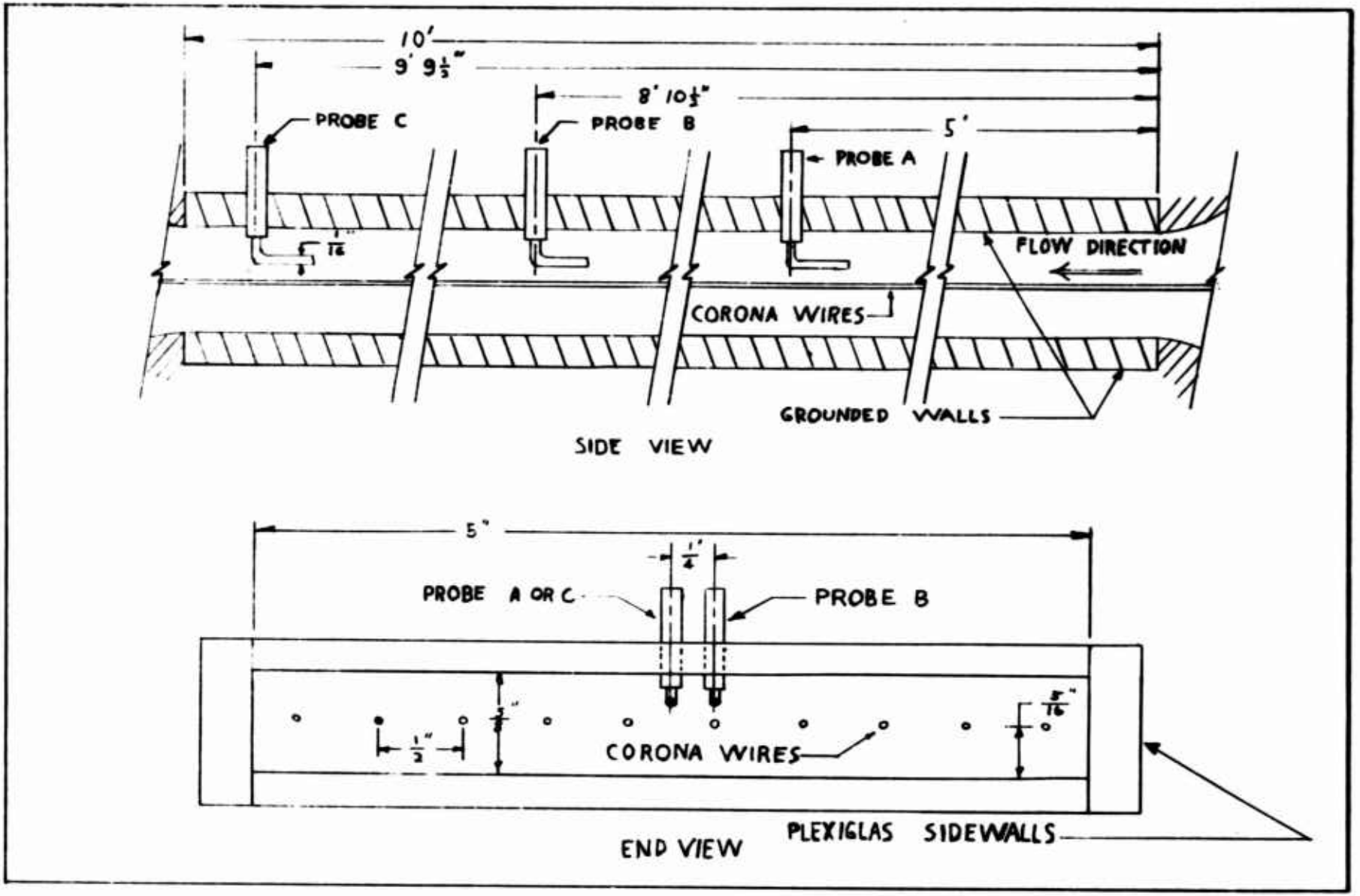

Fig. 3 - Schematic drawing of the flow channel

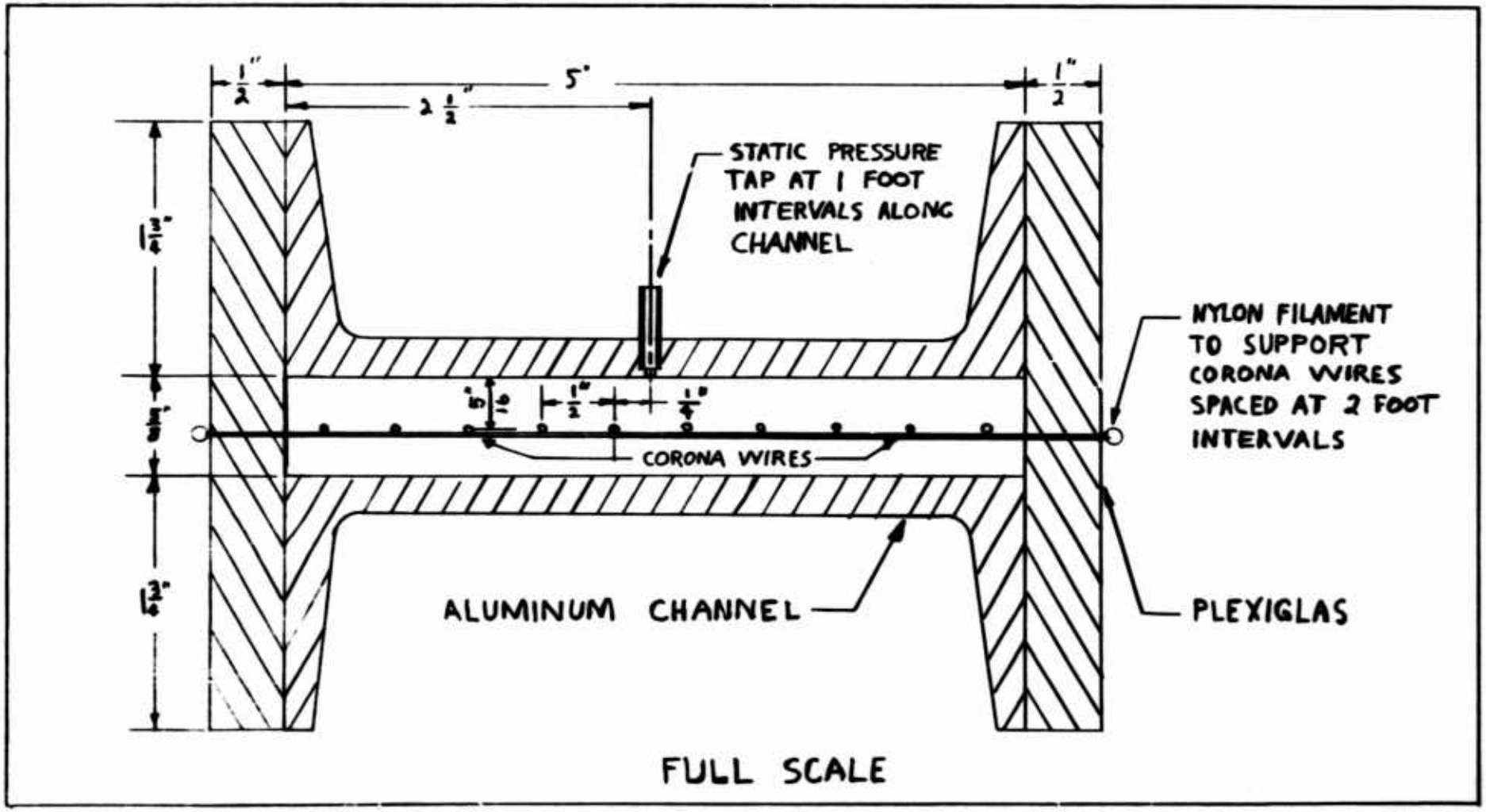

Fig. 4 - Cross sectional drawing of the flow channel

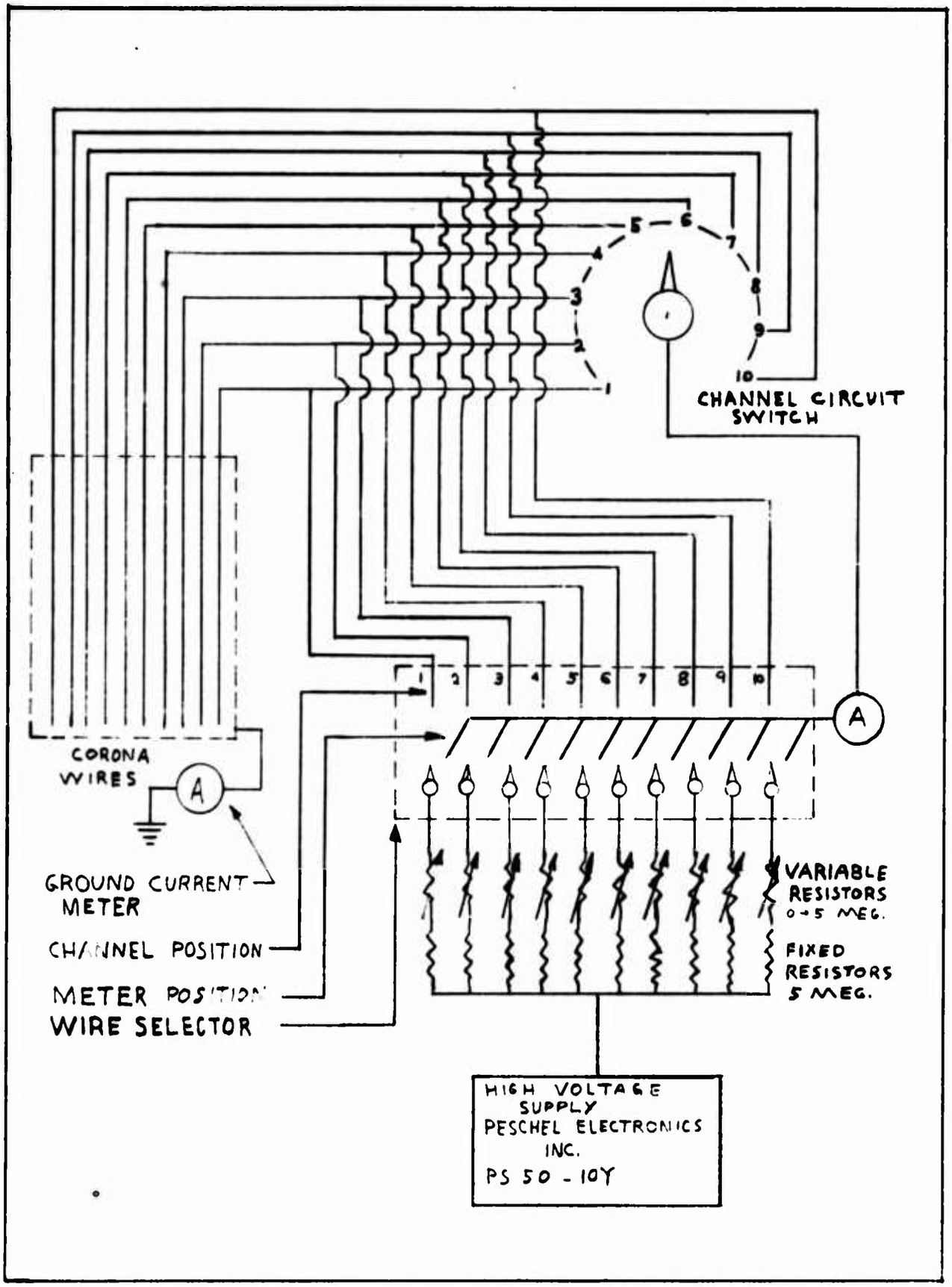

Fig. 5 - Electrical circuit of the flow channel test apparatus

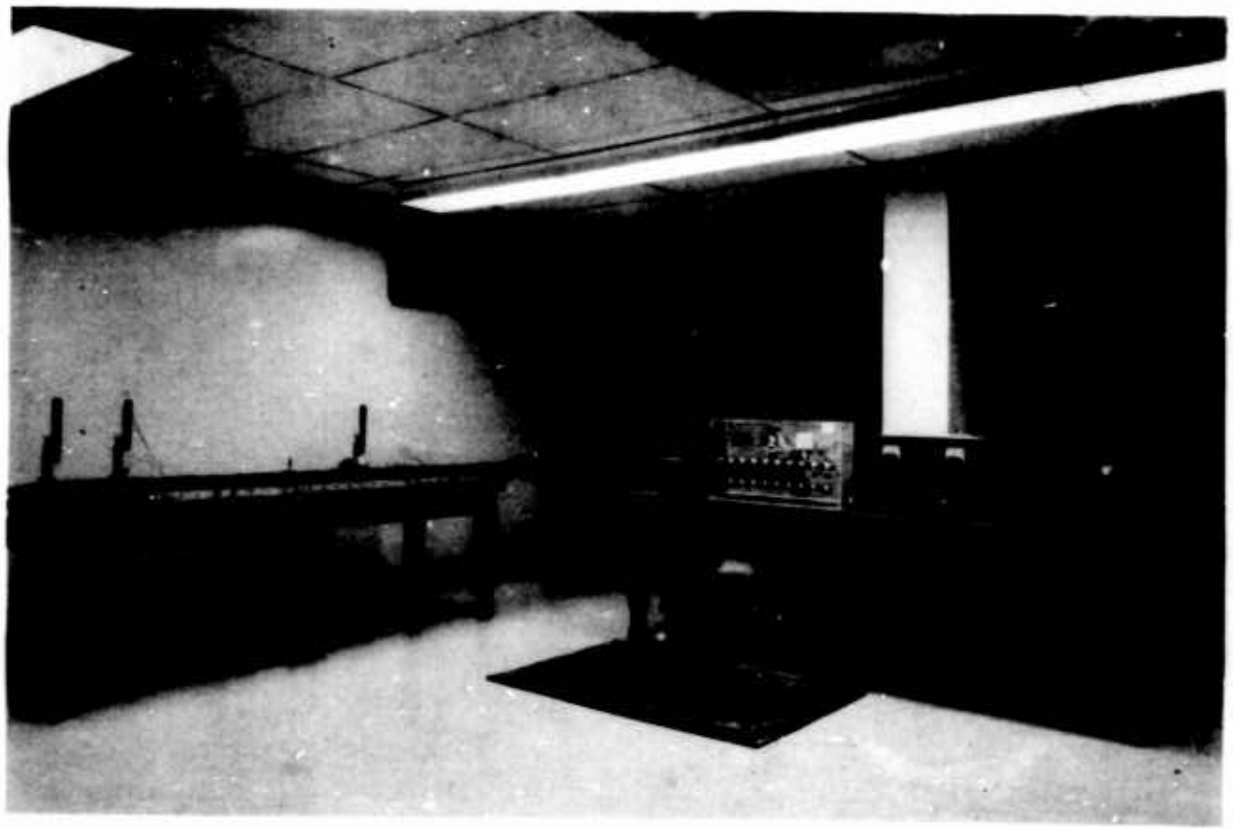

Fig. 6 - Photograph of the flow channel and instrumentation. Channel is on the left. Voltmeter, electrical circuit panel, power supply and micromanometer are on tables.

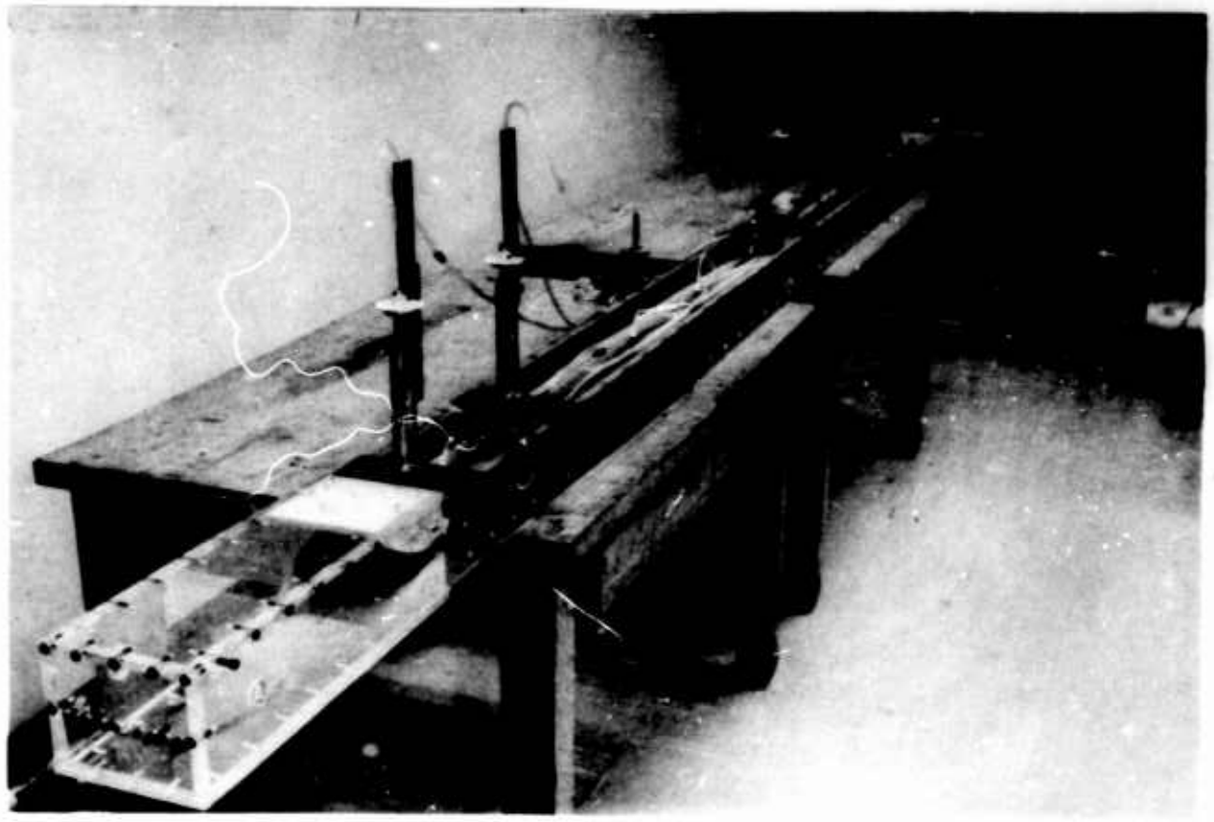

Fig. 7 - Photograph of the flow channel. Dowstream plenum chamber is at lower left. Probe traversing mechanisms are mounted on top wall of channel.

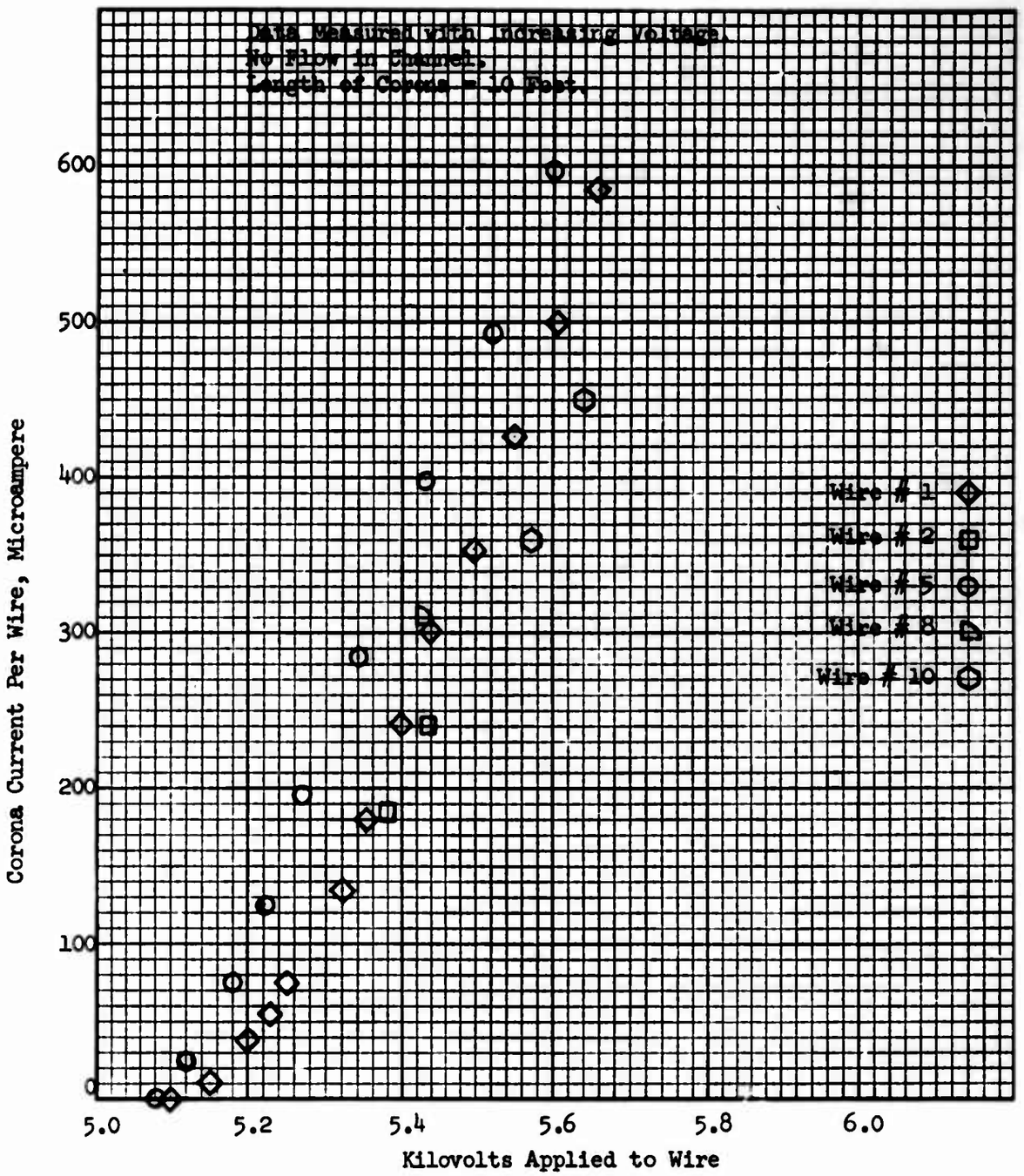

Fig. 8 - Corona current versus volts applied to wire showing the variation in characteristic among the wires

achieved. Figure 8 shows the range of characteristics of the different wires, and Fig. 9 shows the ampere-volts characteristic for ascending the descending voltages.

Figure 10 shows how the ampere-volt characteristic acts with a flow of air in the duct. Since the ampere-volt curves at various Reynolds numbers are approximately identical, it can be concluded that the mean air motion has no effect on the corona voltage-ampere characteristic. It may also be stated that within the range of air flow rates tested, there is no loss of ions by being blown from the duct exit, as this phenomenon would cause the ampere-volt characteristic of the electrical circuit to be dependent on the Reynolds number.

The plane of the ten wires is positioned at the midplane of the channel, and consequently an equal current should flow to each grounded wall if the wire spacing were exact. For the experimental tests performed, it was possible by positioning of the wires to obtain ion currents to the two grounded walls which were equal to within 5%.

Since the approximate theory developed earlier led to the condition that the transverse current density J_y = constant, J_y could be obtained by dividing the total corona current by the total exposed area of both grounded walls. The nondimensional charge numbers as developed earlier by means of various approximations are tabulated below for this flow channel at several values of total corona current.

Total Corona Current in Test Channel	$N\rho_c = \left[\frac{2J_y\epsilon}{HK}\right]^{1/3}\frac{H^2}{\mu K}$	$N_1 = \frac{J_y H^2}{\mu K^2 E_c}$	$N_2 = \frac{J_y H^3}{\mu K^2 V}$
0	0	0	0
1 ma	3.53	0.076	0.343
2.5 ma	5.58	0.1887	0.836
4.0 ma	7.06	0.304	1.31
5.5 ma	8.29	0.415	1.76

It was found that the corona wires, which were bright and lustrous in appearance when new, exhibited a light-brown coating on their surface after an extended period of corona discharge. This phenohenon, postulated to be caused by the corrosive action of ozone, caused a slight change in the volt-ampere characteristics of the wire. As shown in Fig. 11, the effect is to require approximately 150 more volts on the old wire to obtain the same current as on a new wire.

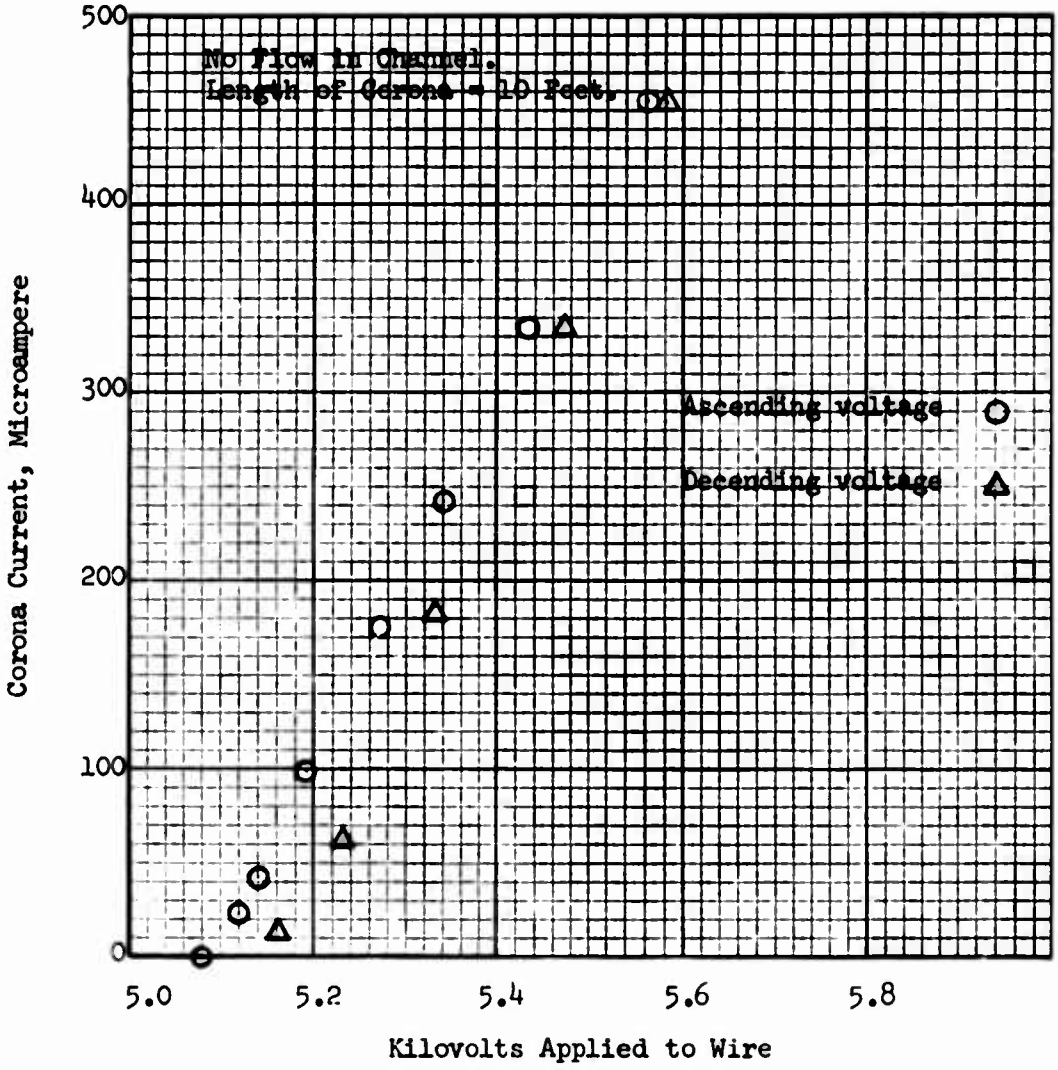

Fig. 9 - Corona current versus volts applied, for wire No. 5, showing the different characteristic for increasing and decreasing voltages

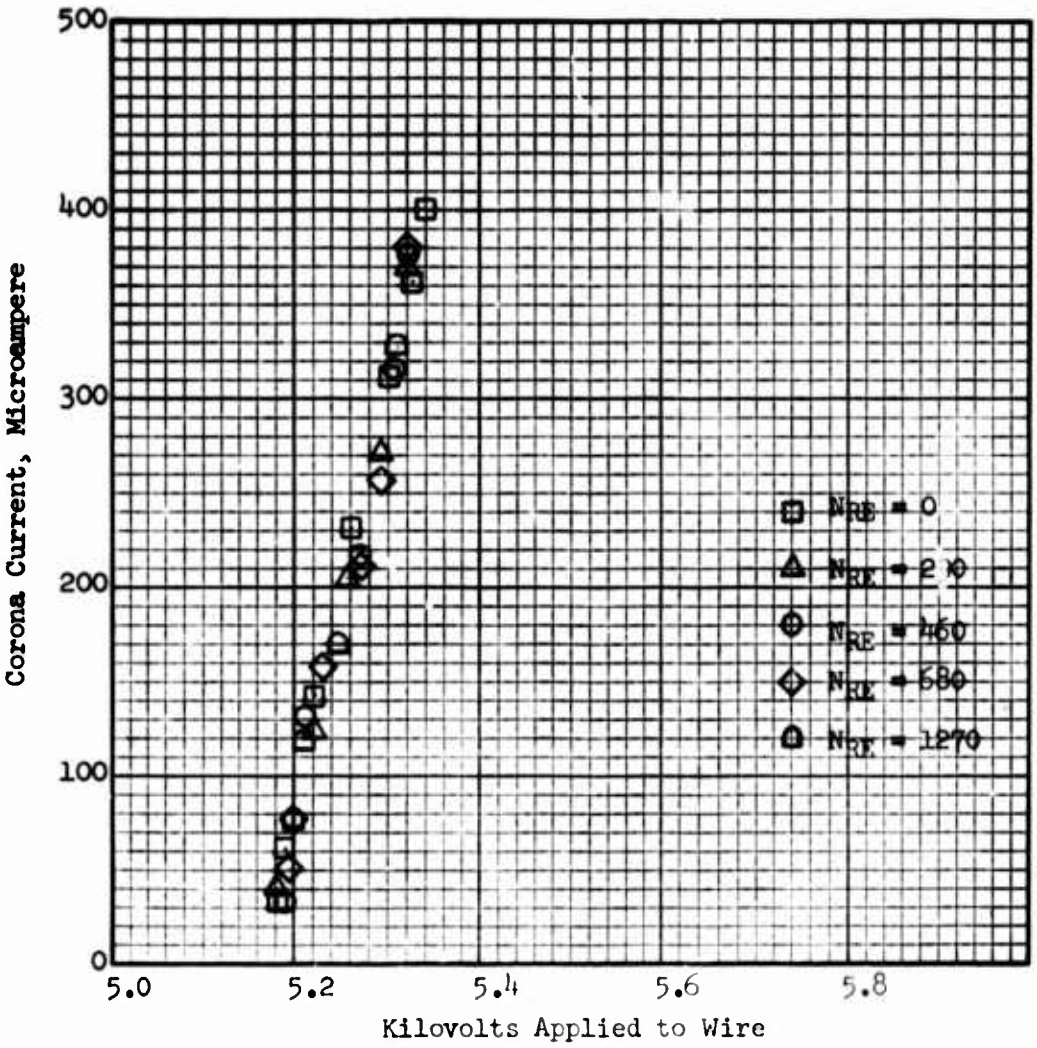

Fig. 10 - Corona current versus volts applied, for wire No. 5, showing that Reynolds number has no effect

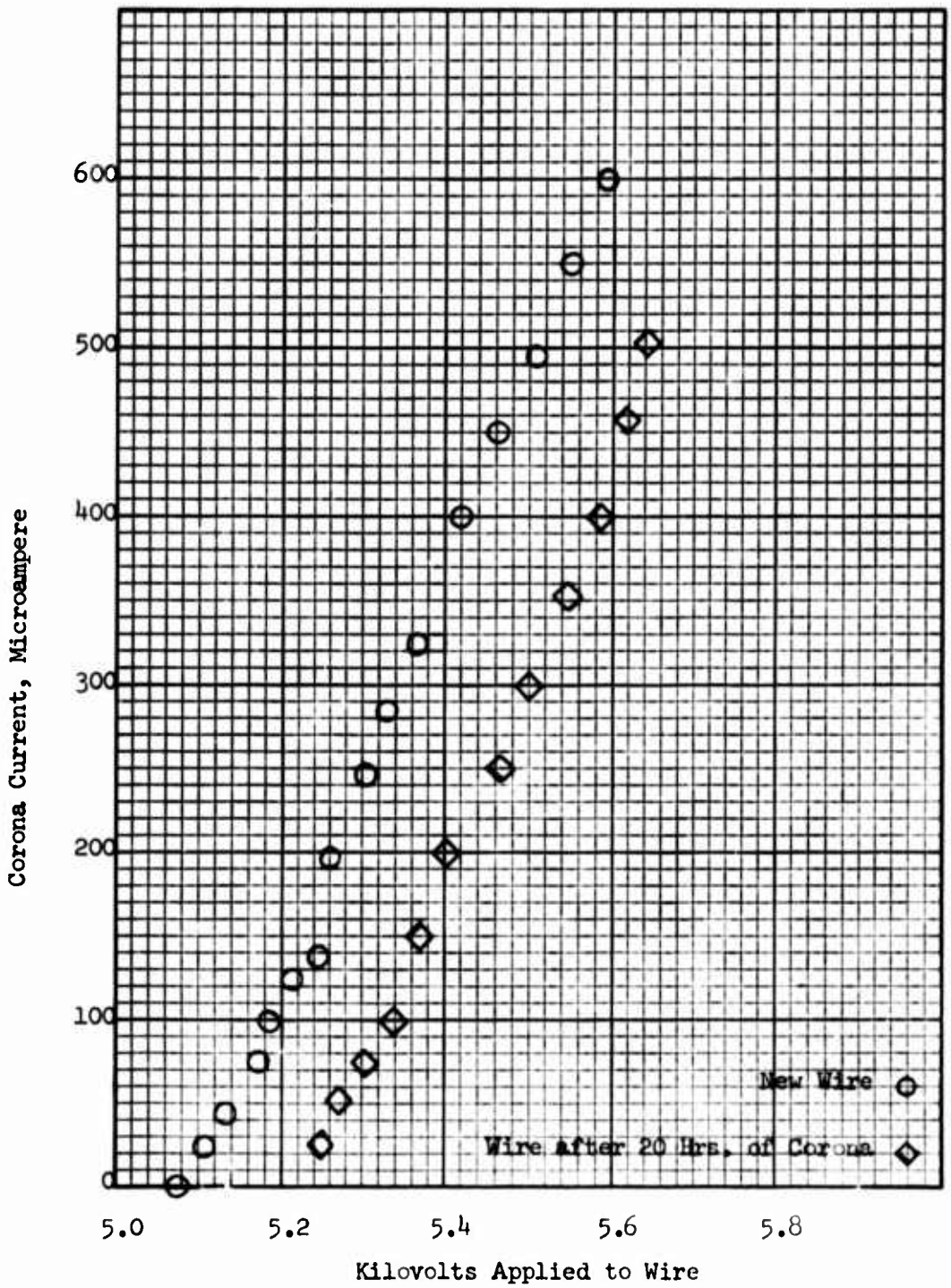

Fig. 11 - Corona current versus voltage applied, for wire No. 5, showing the effect of a period of time on the corona characteristic

Effect of Ions on Friction Factor

A friction factor

$$f = \frac{\frac{\Delta p}{\Delta z} H}{\frac{1}{2} \rho w_m^2} = - \frac{\partial p^*}{\partial \xi}$$

was determined by measuring the static pressure decrease along the duct in the flow direction. It can be seen from Figs. 12, 13, 14, 15, and 16, that the pressure gradient in the flow direction appears as a constant, which supports the assumption that the flow field can be described as "fully established," or one dimensional. Figure 17 shows the log friction factor plotted against log Reynolds number. The curve for zero current is parallel to and slightly above the line $f = 6/N_{RE}$ which is the result for simple laminar flow of air between infinite parallel plates. The amount by which the zero current line is above this curve can be attributed to the side wall and wire influence on the friction, and experimental error.

For Reynolds numbers below about 650, it is seen on Fig. 17 that the curves for friction factor with ion flow are parallel to and above the curve for simple air flow. This indicates that the ion coupling effect behaves as a laminar flow, i.e., friction factor times Reynolds number equals a constant for a certain charge number $N\rho_c$.

Above Reynolds numbers of about 650, the curve in Fig. 17 for zero current departs from linearity, indicating transition to turbulence. The flow regime above $N_{RE} = 650$ will therefore be considered the turbulent regime. It is noted from Fig. 17 that within the turbulent regime the measured friction factors with ion current fall on the same curve as the flow with no ion current. In this flow regime the frictional resistance caused by turbulent mixing becomes large in relation to the induced electric body force, and thus would tend to overshadow the measureable effect of the charge number. In addition, the eddy diffusivity associated with turbulence might sufficiently affect the ion distribution across the duct to result in smaller electric body force than would exist in laminar flow at the same charge number.

The quantitative effect of ion current on the friction factor is depicted in Figs. 18 and 19, which include only data in the laminar flow regime. Also included on Fig. 18 are curves representing the approximate solutions developed earlier (Eqs. (30, 33, 39, 44). All the theoretical curves have been shifted upward on Figs. 18 and 19 by a facotr of 1.53 so that they agree with the experimental friction factor data at zero ion current. This upward shift represents the friction contributed by the side walls of the channel and the corona wires-- not included on the theoretical treatment, as well as systematic experimental errors.

Figure 18 shows that the experimental data lie between the first two and last two of the approximate solutions listed on page 11. The upper two curves, Eqs. (30) and (33) are functions of $N\rho_c$, which contain the ion current to the

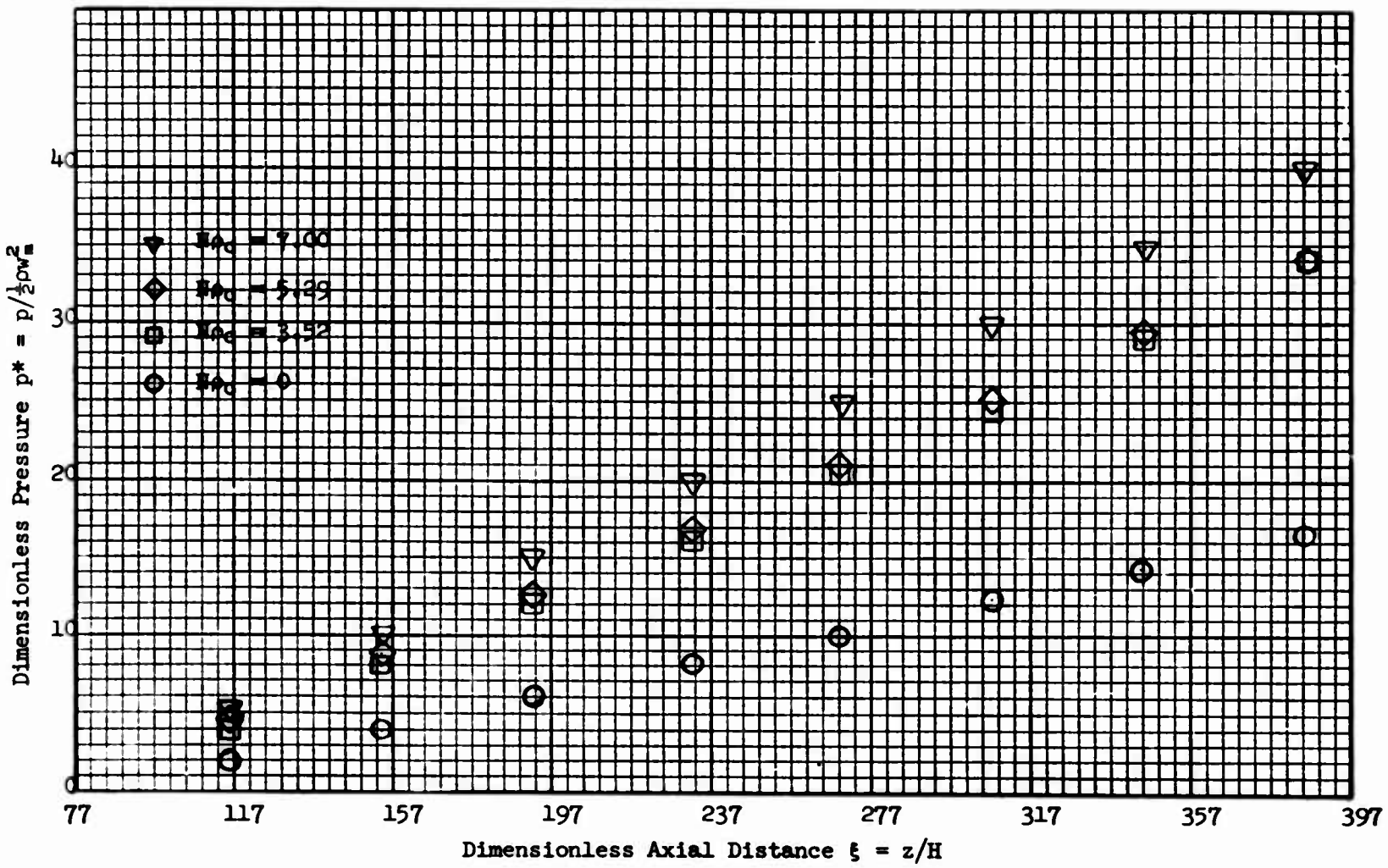

Fig. 12 - Nondimensional static pressure versus distance along duct for a Reynolds number of approximately 140, with charge number as parameter

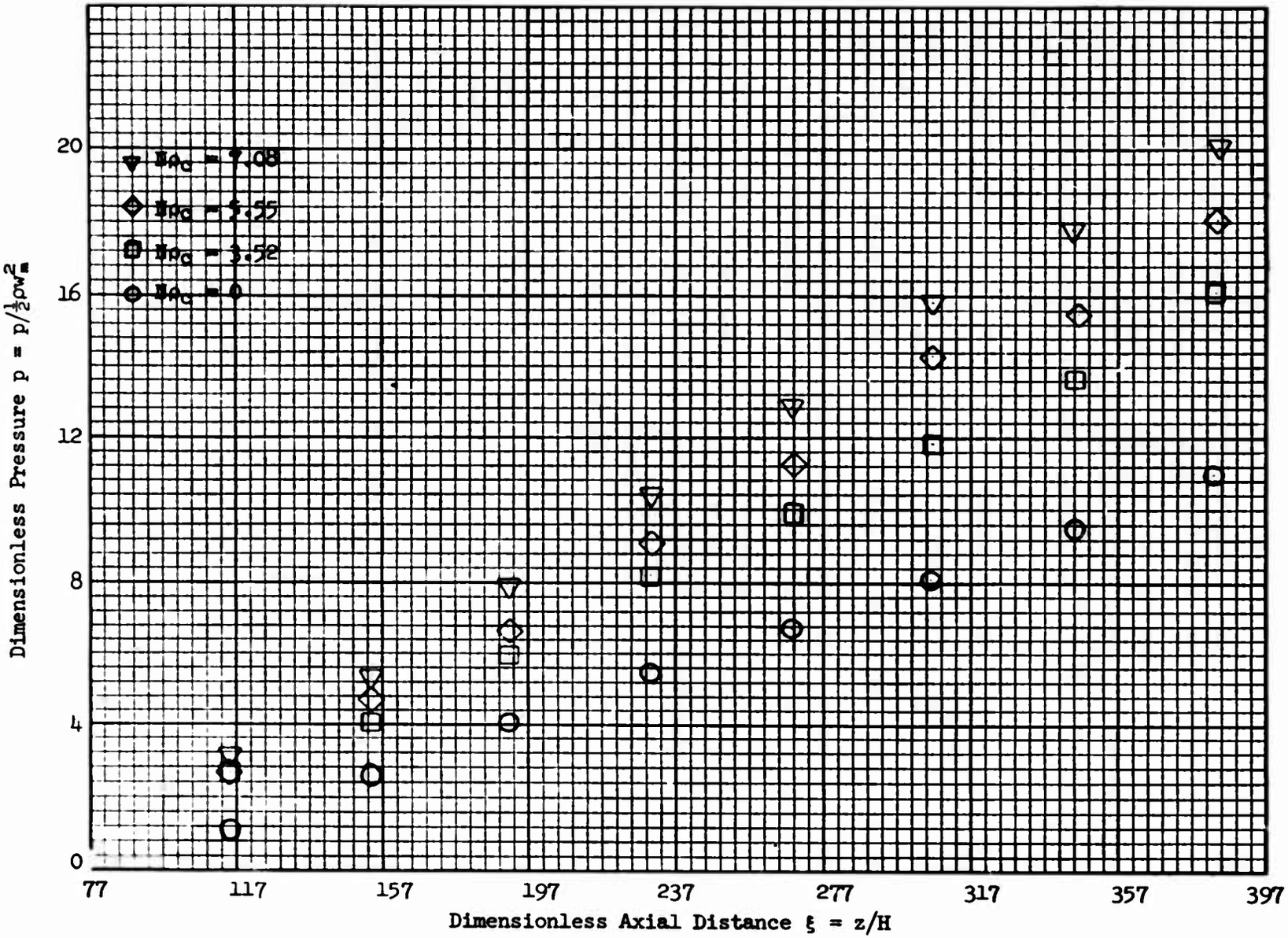

Fig. 13 - Nondimensional static pressure versus distance along duct for a Reynolds number approximately 265, with charge number as parameter

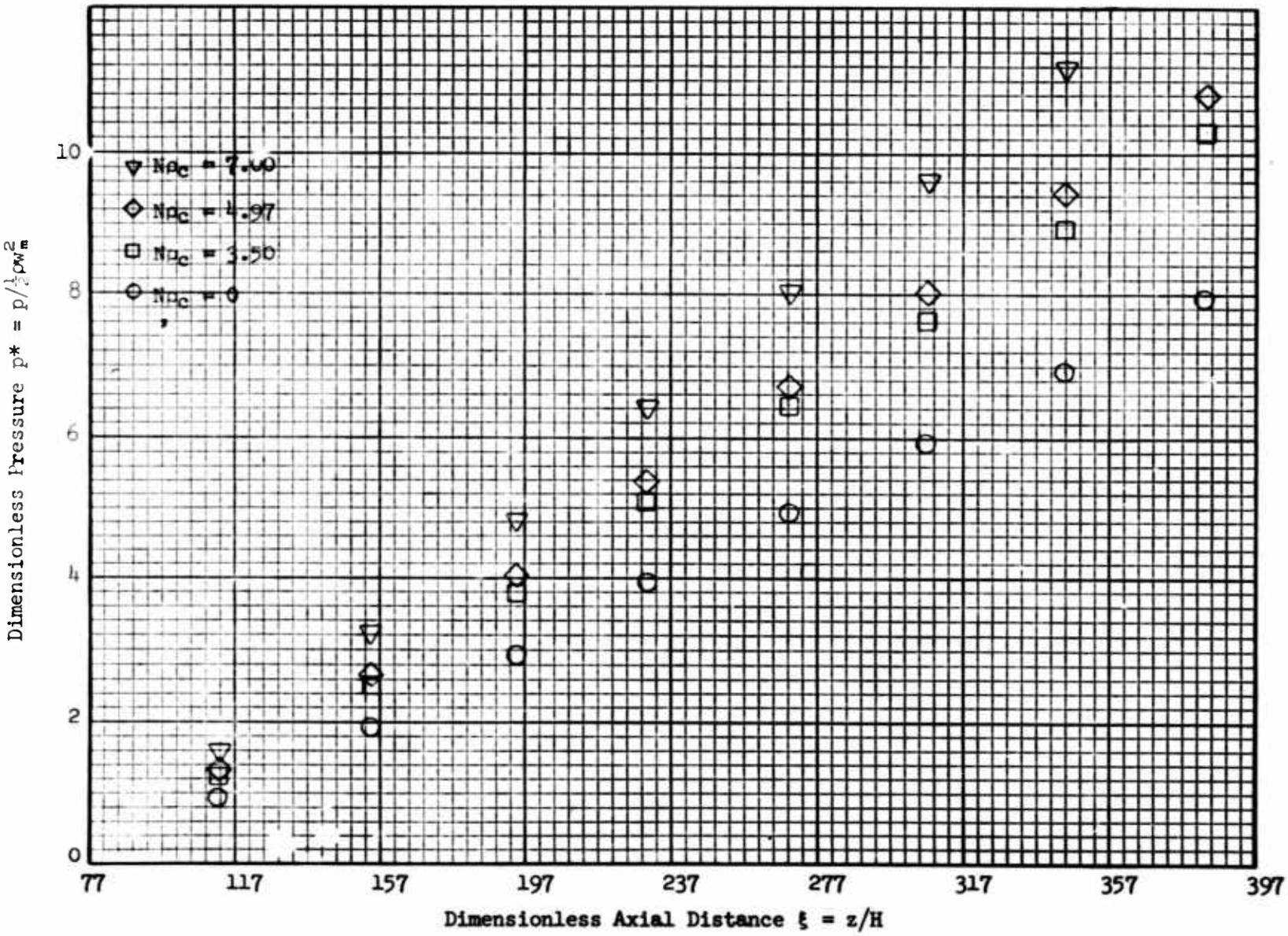

Fig. 14 - Nondimensional static pressure versus distance along duct for a Reynolds number of approximately 400, with charge number as parameter

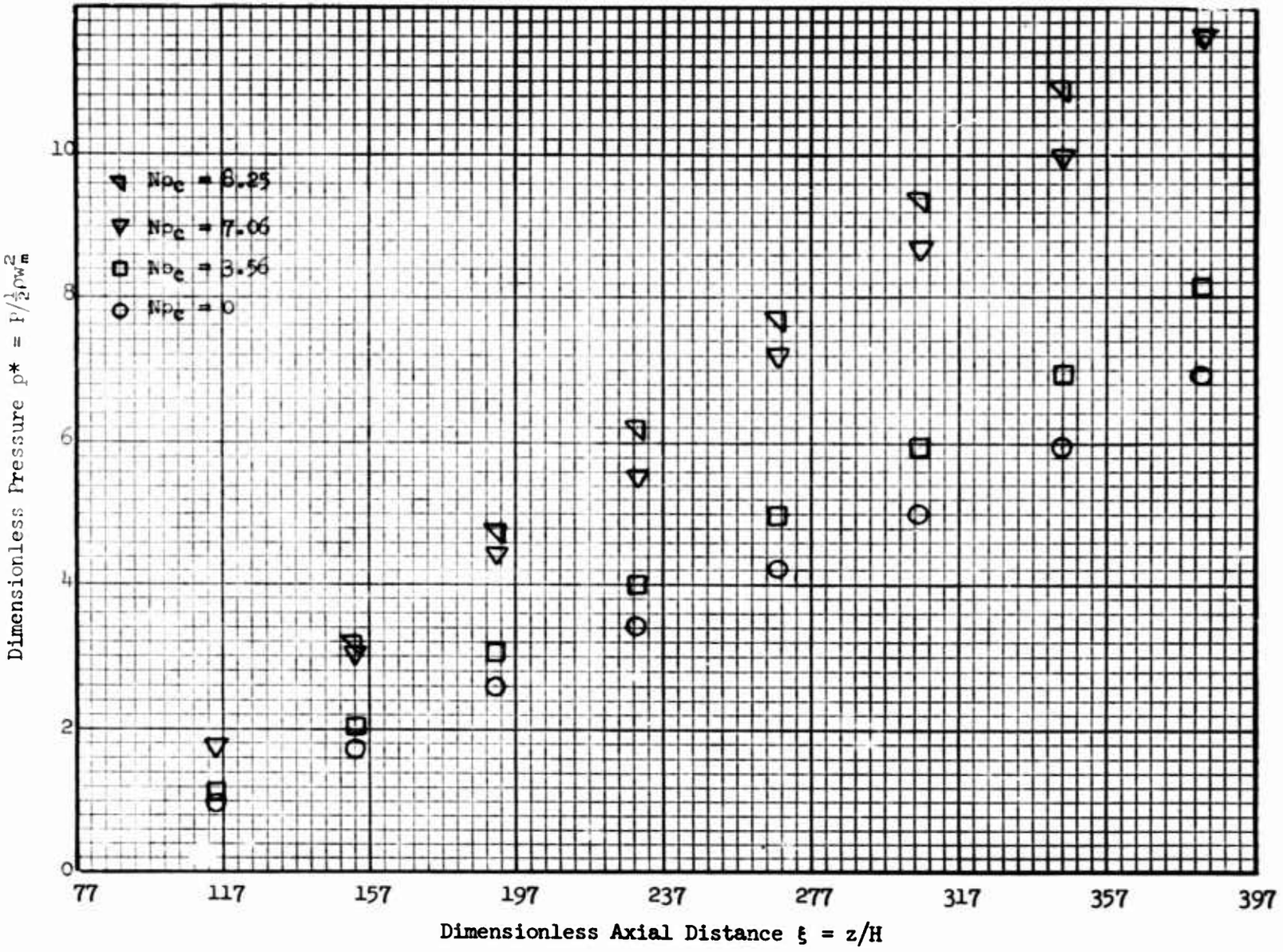

Fig. 15 - Nondimensional static pressure versus distance along duct for a Reynolds number of approximately 540, with charge number as parameter

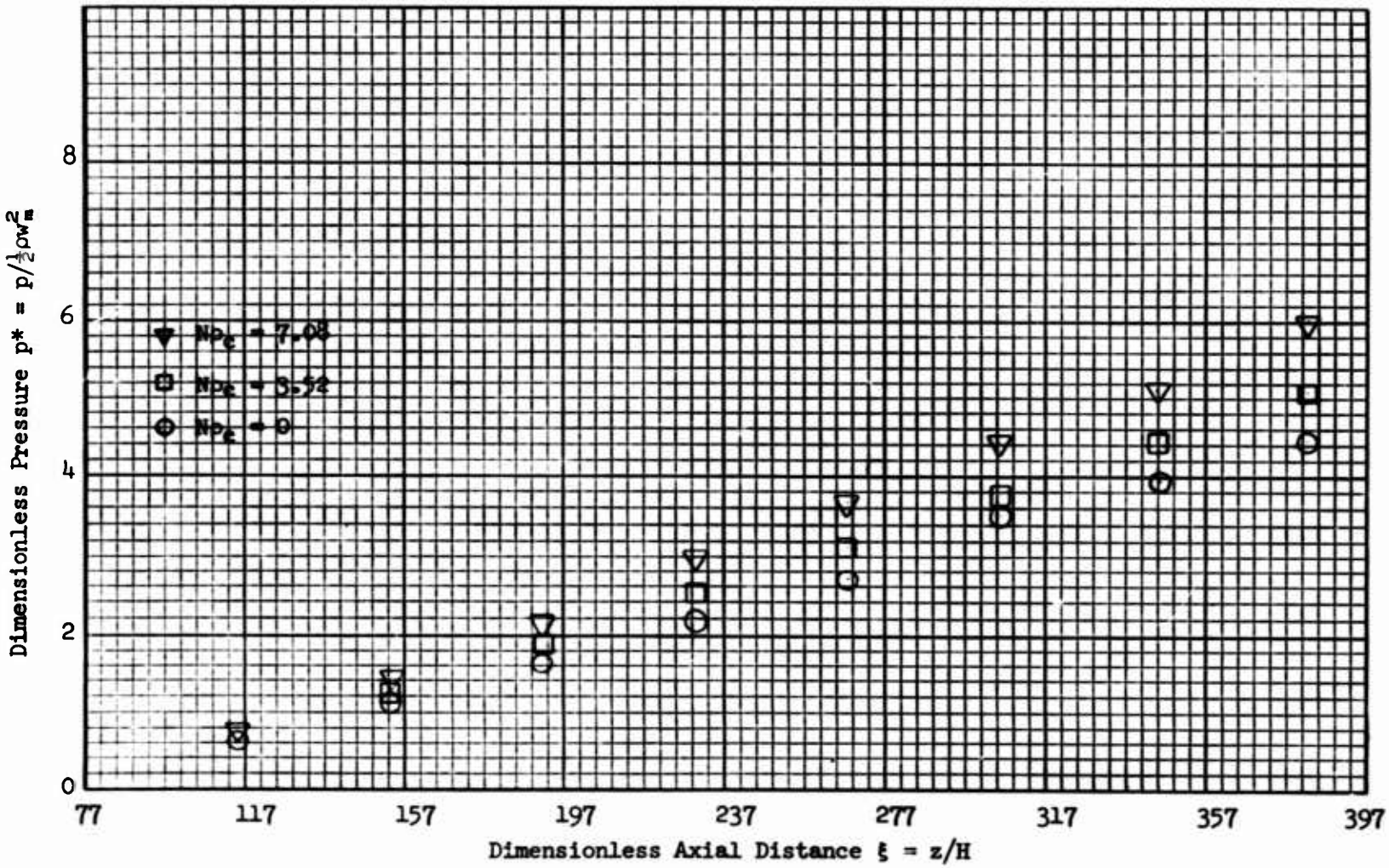

Fig. 16 - Nondimensional static pressure versus distance along duct for a Reynolds number of approximately 1100, with charge number as parameter

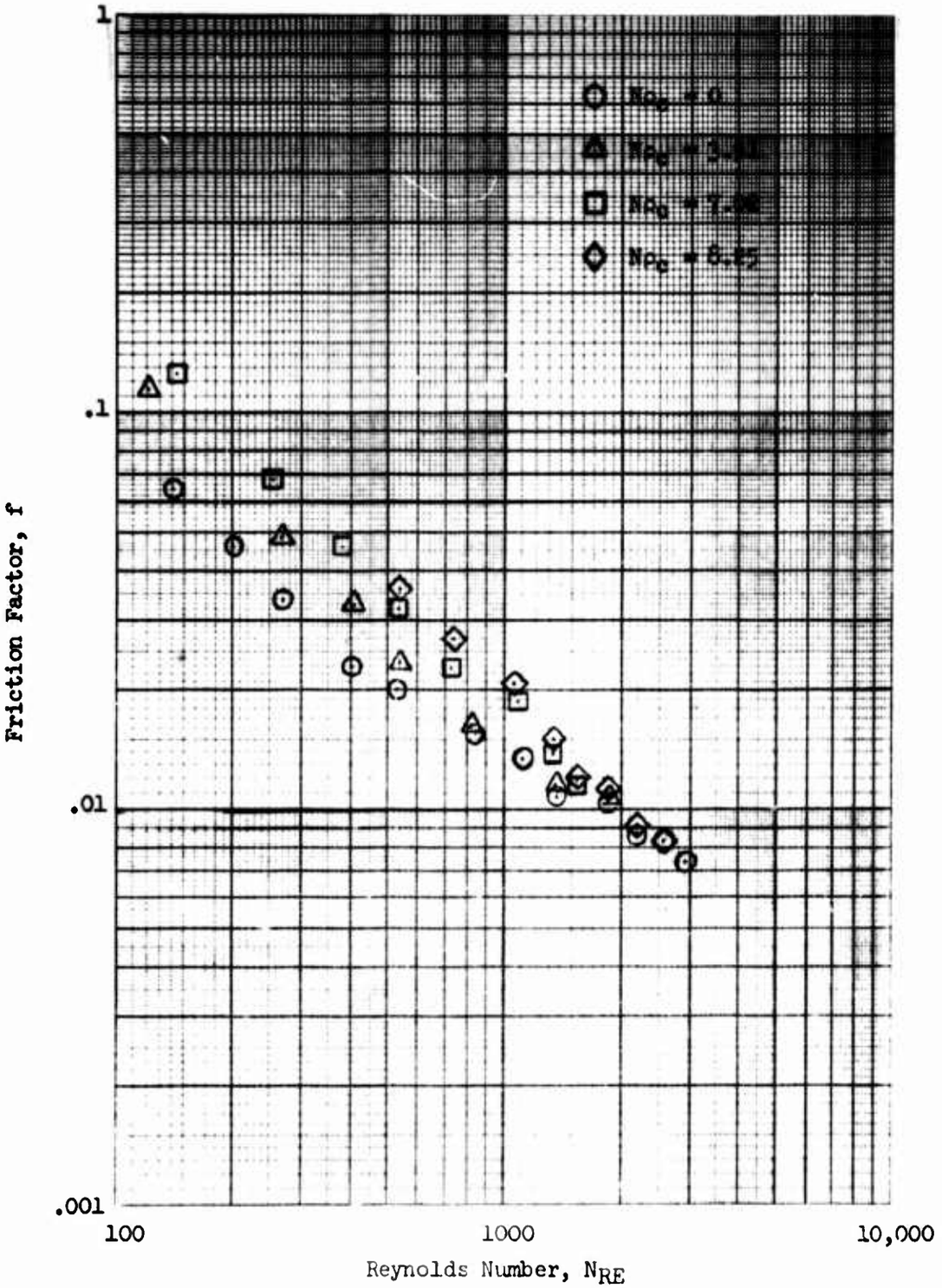

Fig. 17 - Log friction factor versus log Reynolds number, with charge number as parameter

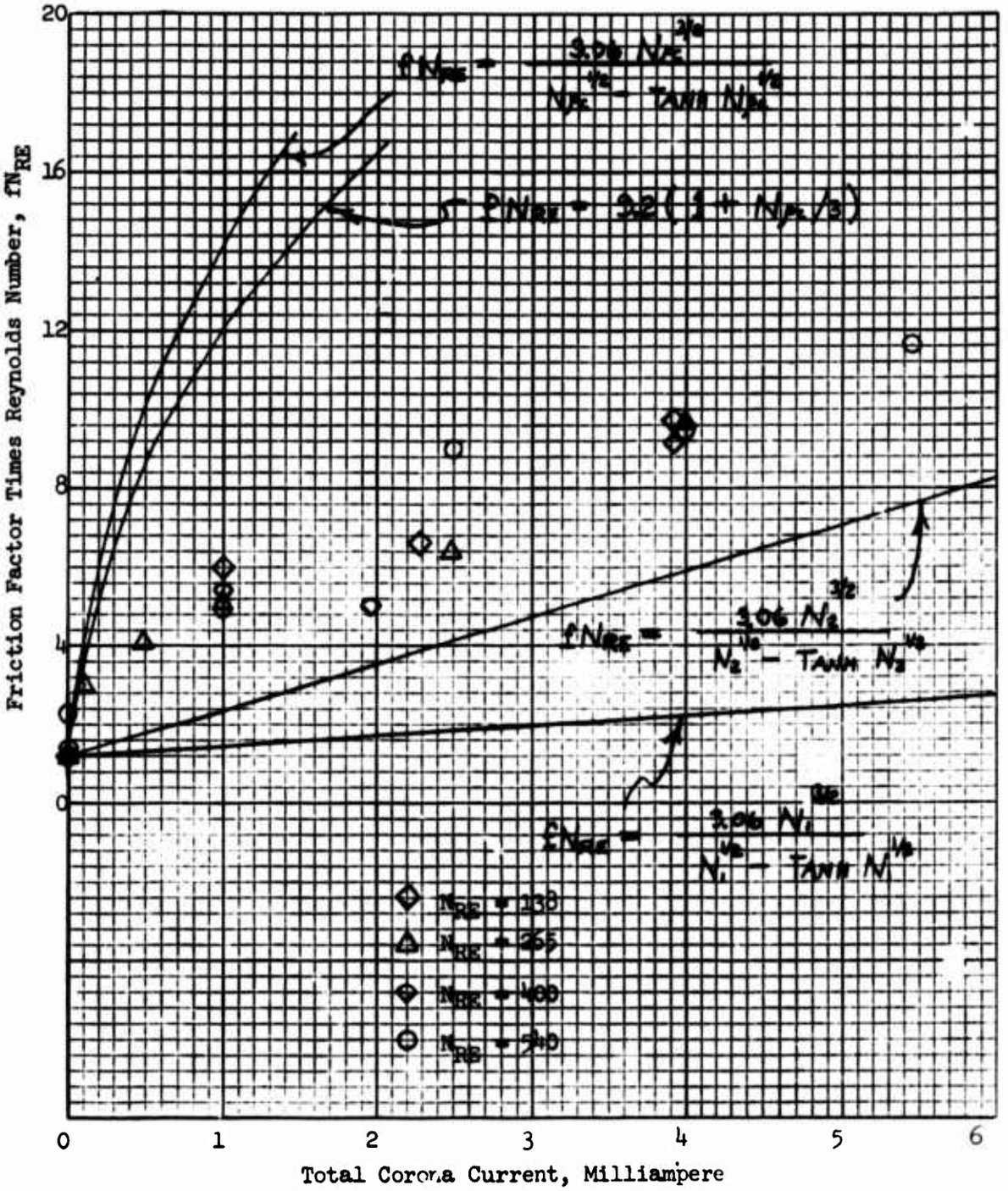

Fig. 18 - Friction factor times Reynolds number versus total corona current showing comparison between experiment and theoretical models

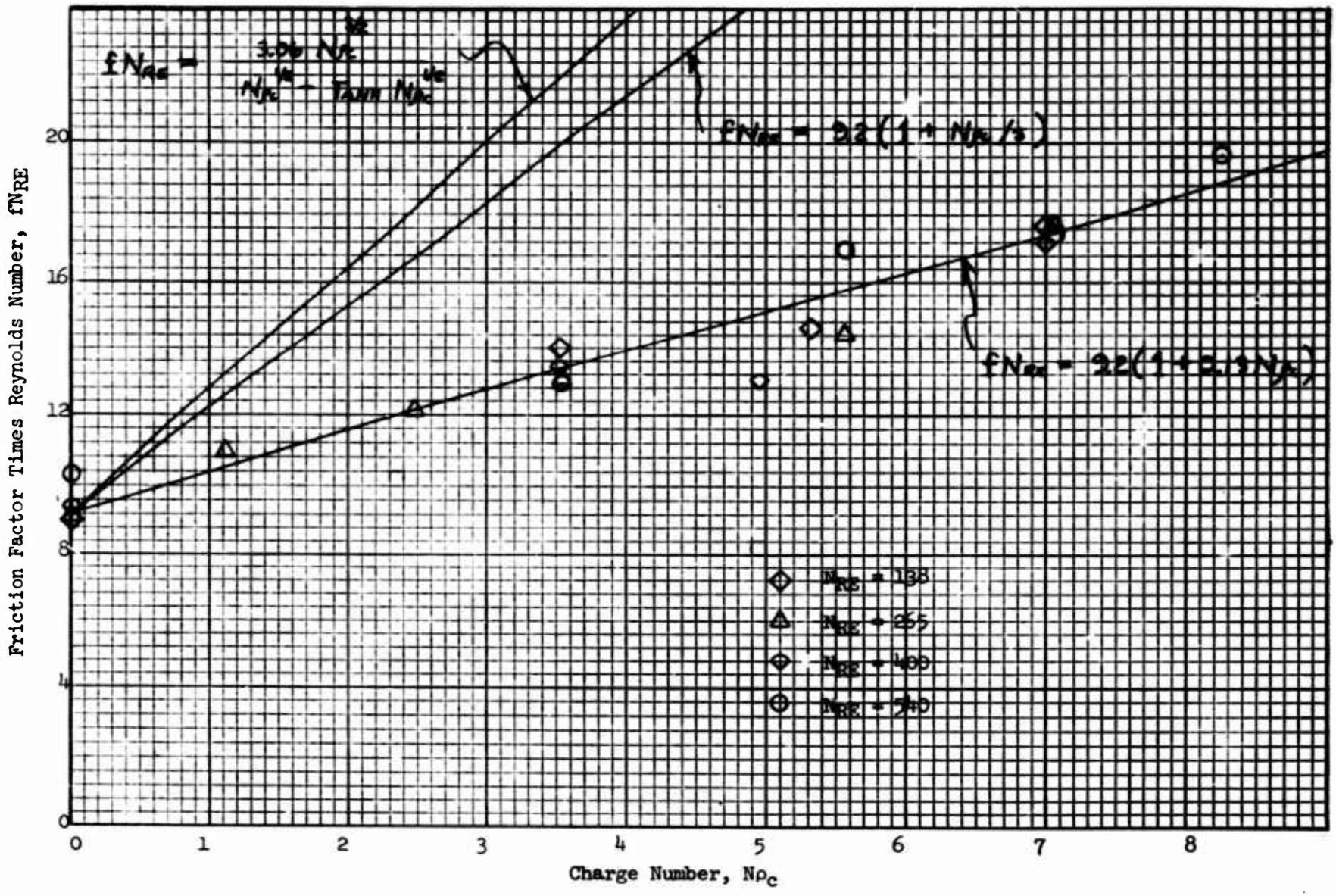

Fig. 19 - Friction factor times Reynolds number versus charge number, showing comparison between experiment and a theoretical model

one-half power, and hence appear as curved lines. The lower curves, Eqs. (39) and (44) are functions of N_1 and N_2 which contain the ion current to the first power, and hence appear as approximately straight lines. Although Eq. (44) is closest to the data points at high values of current, it is to be noted that the data functionally does not behave as a straight line for small values of current.

On Fig. 19 the experimental friction factor data is plotted against $N\rho_c$. It is seen that the data fall fairly well on a straight line for all values of charge number, and hence it is concluded that the friction factor is functionally dependent on the ion current to the one-half power. Although the theoretical curves on Fig. 19 indicate much too great on ion effect than that measured, it must be remembered that they are dependent on the value of the mobility, which appears in the charge number to the 3/2 power, and the exact value of mobility to be used in any one experiment is somewhat uncertain.[5] A straight line was drawn through the data points on Fig. 19 which represents

$$fN_{RE} = 9.2\ (1 + 0.13\ N\rho_c), \tag{51}$$

an empirical line which best fits the experimental data.

Effect of Ions on Transverse Pressure Gradient

For fully established flow with no ion effect, the static pressure transverse to the flow is constant. However, in the presence of a field E_y and a charge density ρ_c, there results a body force in the transverse (y) direction equal to $\rho_c E_y$, which, for one dimensional flow is equal to the transverse pressure gradient, $\partial p/\partial y$.

Since

$$\frac{\partial J_y}{\partial y} + \frac{\partial J_z}{\partial z} = 0$$

from Eq. (6) and J_z was assumed zero, there results

$$J_y = \rho_c K E_y = \text{constant} \tag{52}$$

and since $\rho_c E_y = \partial p/\partial y$ from Eq. (11) then

$$\frac{\partial p}{\partial y} = \frac{J_y}{K} = \text{constant}. \tag{53}$$

Static pressure measurements were made using the traversing pressure probes with zero air flow in the duct. Figure 20 shows the pressure variation at locations A and C which represent traverses between corona wires. It is seen from the slopes of the curves that the experimentally measured pressure gradient is approximately equal to the theoretical gradient except for a region near the wires representing about one-fourth of the duct volume. In this region the fact that there are discrete wires, each acting as an ion emitting plume, may be affecting the pressure variation. Therefore it can be expected that the transverse pressure gradient near the plane of the wires will be somewhat different from the gradient far from the wires. It is also noted that the pressure distribution at location C, near the duct exit, is similar to the distribution at location A, as expected since the probe locations only differ in the value of axial position z.

It was thought that the transverse pressure gradients existing in the channel could result in a circulating flow around the corona wires, (corona wind) which would also have the effect of increasing the friction factor if the circulation were active with an axial flow. Therefore, transverse pressures with no net axial flow were measured with the pressure probe oriented along the axis (the total pressure probes used in the flow tests) and also with a probe oriented perpendicular to the bottom duct wall. If there was any air movement in the duct, there would be a different pressure distribution read by the probes in the two orientations. Figure 21 shows a comparison of the pressure measurements made at location A, which shows some scatter, but no definite differences in the pressure distribution as measured by probes at the two orientations. For all the pressure measurements at locations A and C, the minimum pressure was at $\eta = \pm 0.2$ to ± 0.3, this fact not explicable by a model of a planar ion source may be caused by the effect of the individual wires.

Figure 22 shows the pressure distributions measured at location B, which is located directly above a wire. Again there is some scatter in the measurements, and it is not evident that the probe orientation is important here. The data points indicate that the pressure distribution does not follow the slope of the theoretical $\partial p/\partial y = J/K$ line. It is suspected that here, when the probe is directly over the wire, the presence of the probe affects the corona discharge and hence affects the ion density in the vicinity of the probe. Figure 23 shows the effect of current on the transverse electric pressure difference between the point $\eta = -0.5$, which is halfway between the midplane and the lower wall, and the pressure at the upper wall, where $\eta = 1$. The measurements show an approximately linear increase of pressure with current density, as expected, and the slope of the data points is approximately equal to the theoretical line based on $\partial p/\rho y = J_y/K$.

Effect of Ions on Velocity Distribution

Local velocities across the air duct were determined at locations A, B, and C, by measuring the difference between the total pressure and the static pressure. The total pressure was measured with a glass probe oriented upstream. The static pressure at the upper wall at locations A, B, and C were

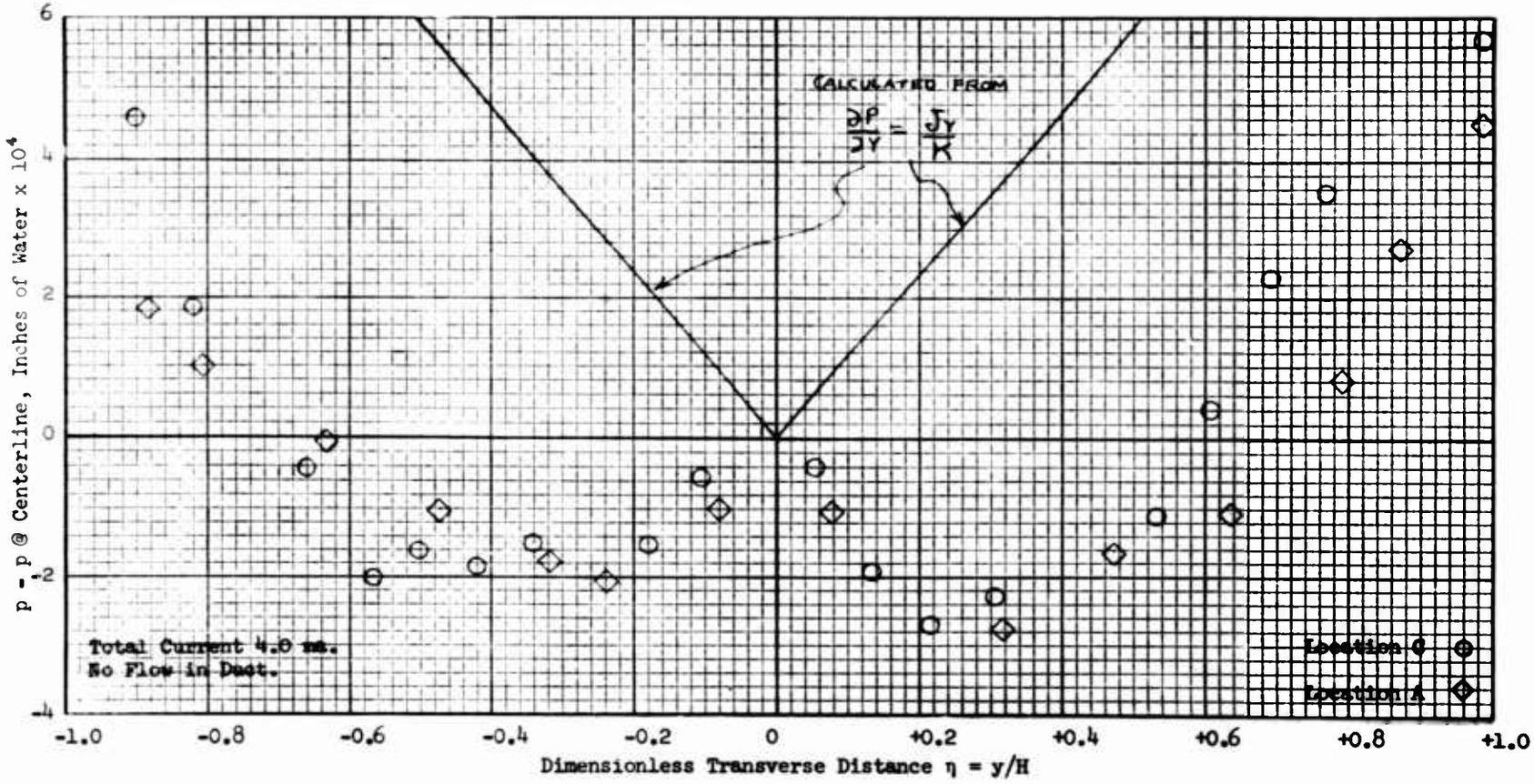

Fig. 20 - Electric pressure versus nondimensional transverse distance, η, for location A and C

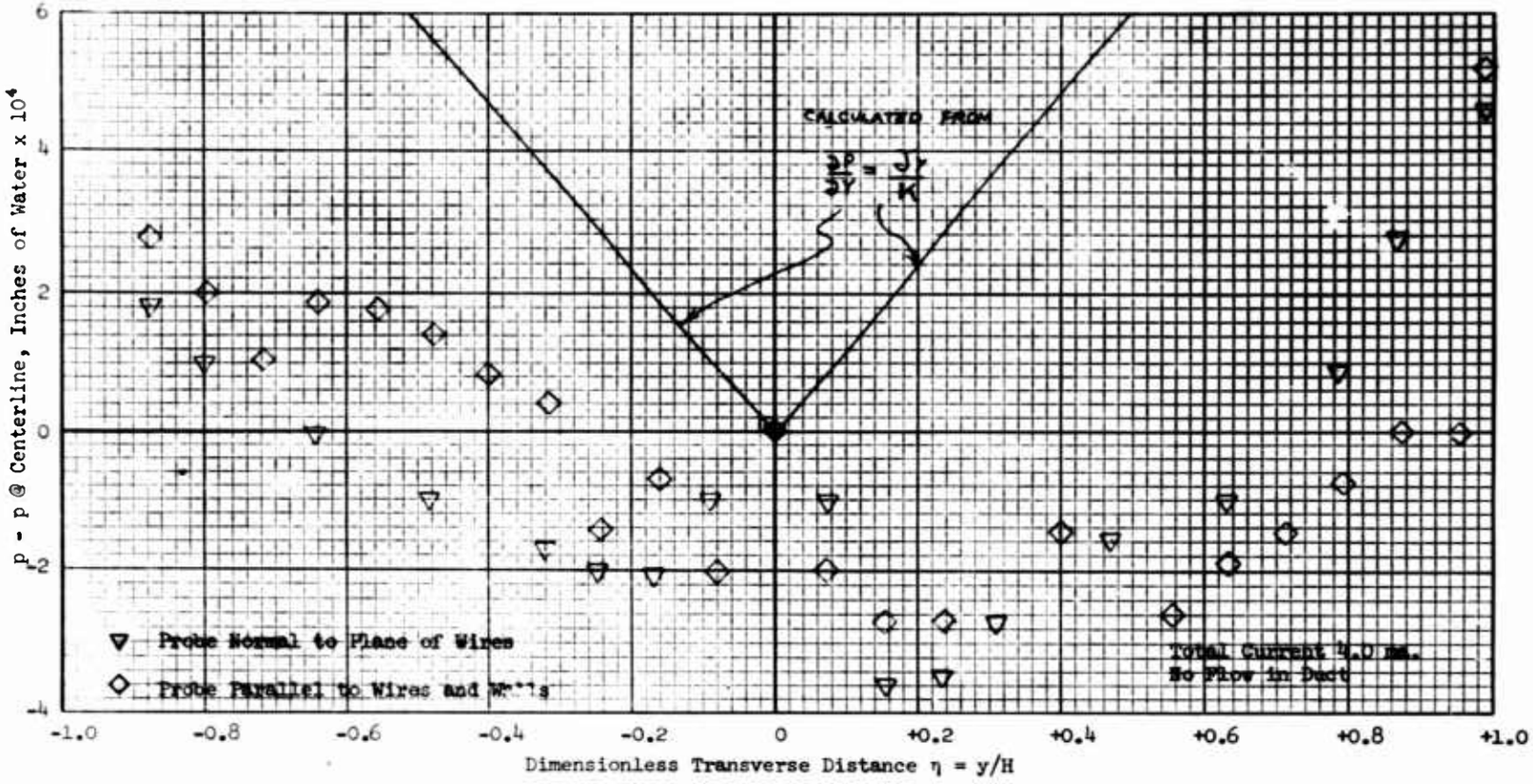

Fig. 21 - Electric pressure versus nondimensional transverse distance, η, for location A for two different probe orientations

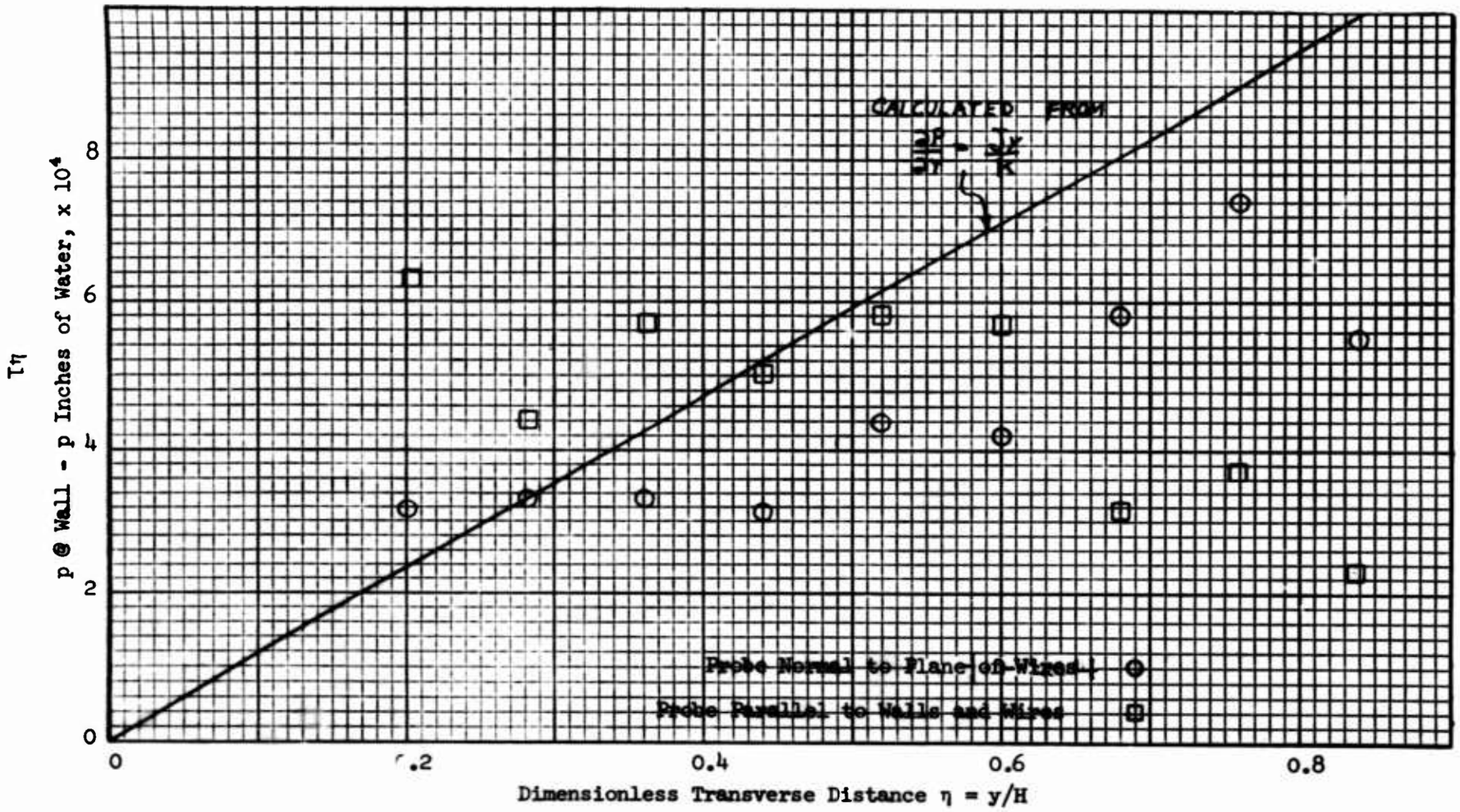

Fig. 22 - Electric pressure versus nondimensional transverse distance, η, for location B

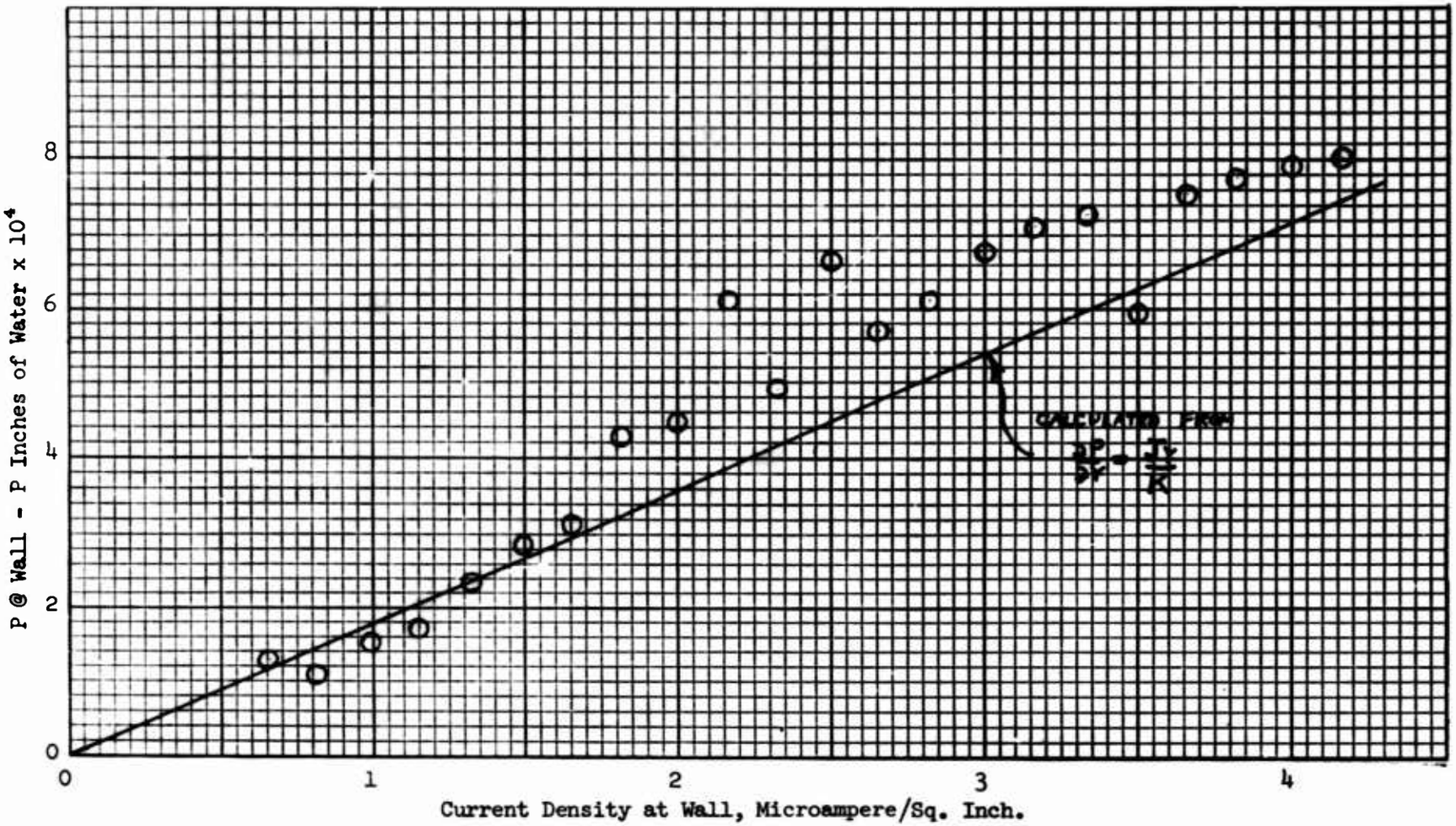

Fig. 23 - Difference between pressure at wall and probe pressure at $\eta = .5$ versus corona current density

obtained from the pressure at a point away from the wall was then determined from the transverse electric pressure curves of Figs. 20 and 22. Since no correction was made for the effects of sheared flow on the static probe reading near the wall or wire, errors can be expected for the velocity determination close to the wall or wire; also, because of the large scatter in the transverse pressure gradient measurements, the velocity profile data are subject to a large experimental error.

Figure 24 shows the results of velocity determination for location A compared with the velocity profile determined by the approximate theory. The mean velocity w_m used to nondimensionalize the velocity was determined by a measurement of the total flow in the duct. The integrated value of the velocity curve over the flow cross section should, therefore, equal 1.0 if no experimental erros existed. The effect noticed is that the experimentally measured velocity profile is flattened much more than the theoretical model would indicate.

The velocity curves for low Reynolds numbers, Figs. 25, 26, 27 in the laminar regime, show that the ion coupling acts to depress the velocity at the center of the duct and causes a higher velocity gradient (and more friction) near the walls, in qualitative agreement with the approximate theory. Near the center of the duct the deviation of the theoretical velocity curve and the measured values is the greatest, but it is here that the effect of the discrete corona wires affect the model, as discussed earlier in the treatment of the transverse pressure gradient.

The velocity curves for a flow rate in the turbulent regime, Fig. 27 shows that the ion effect is very small, in agreement with the effect noticed on the friction factor, that the ion effect was small in the turbulent regime.

Figure 28 is the measured velocity distribution at location B, which shows an almost flat profile. As discussed earlier in connection with the transverse electric pressure at location B, the electric pressure determination here is in doubt because of the probe effect on the local corona discharge. The velocity determination at location B is therefore thought to be much more in error than at locations A and C where the probes are between wires. Figure 29 is a measured velocity distribution at location C, near the end of the duct, and is seen to be similar to the results obtained at location A.

Effect of Flow on Current Density

From the electrical field equations,

$$\nabla \times E = 0 \tag{54}$$

and in this channel case this equation reduces to Eq. (7)

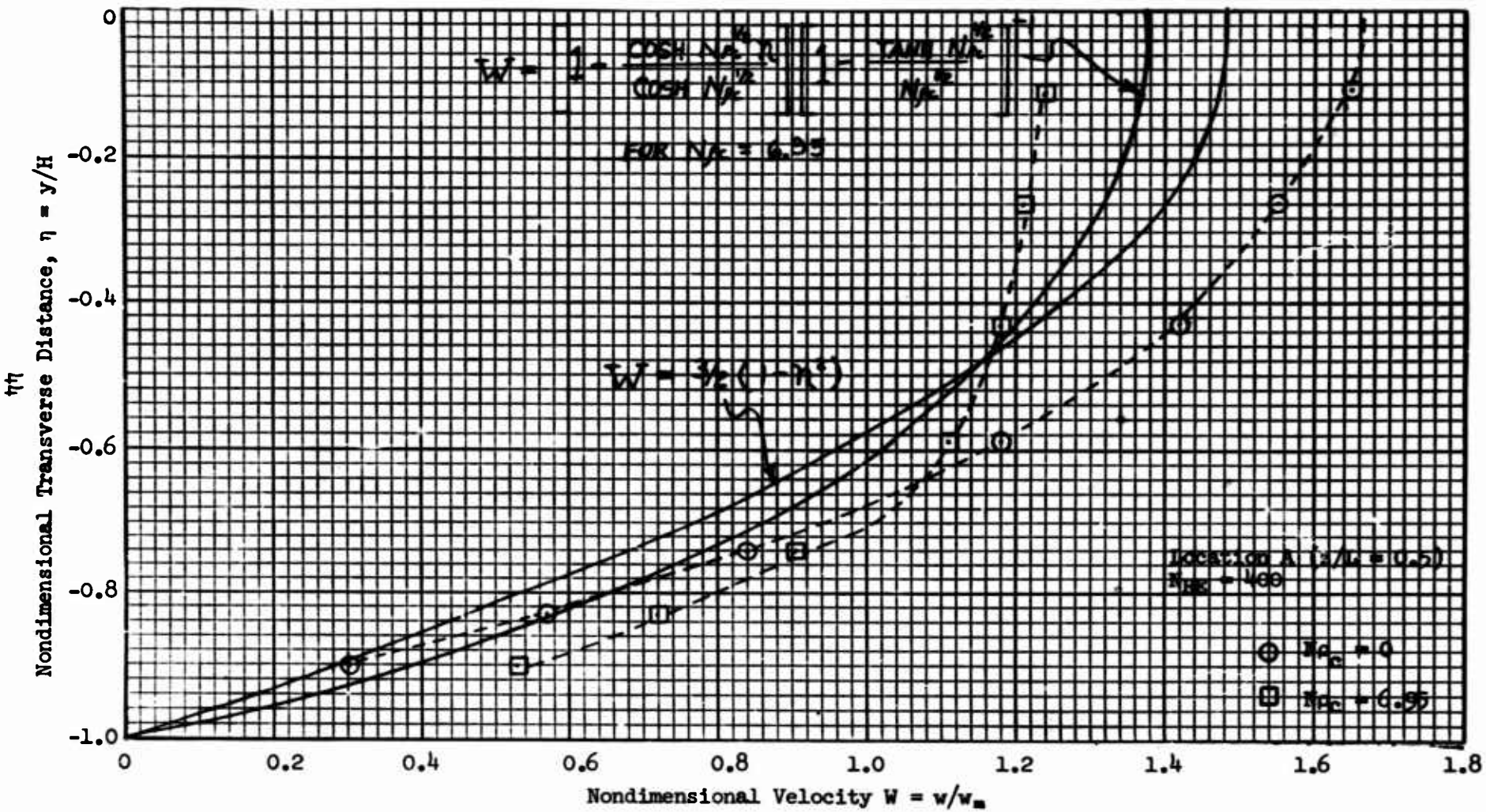

Fig. 24 - Nondimensional velocity profile, comparing experimental data with a theoretical model

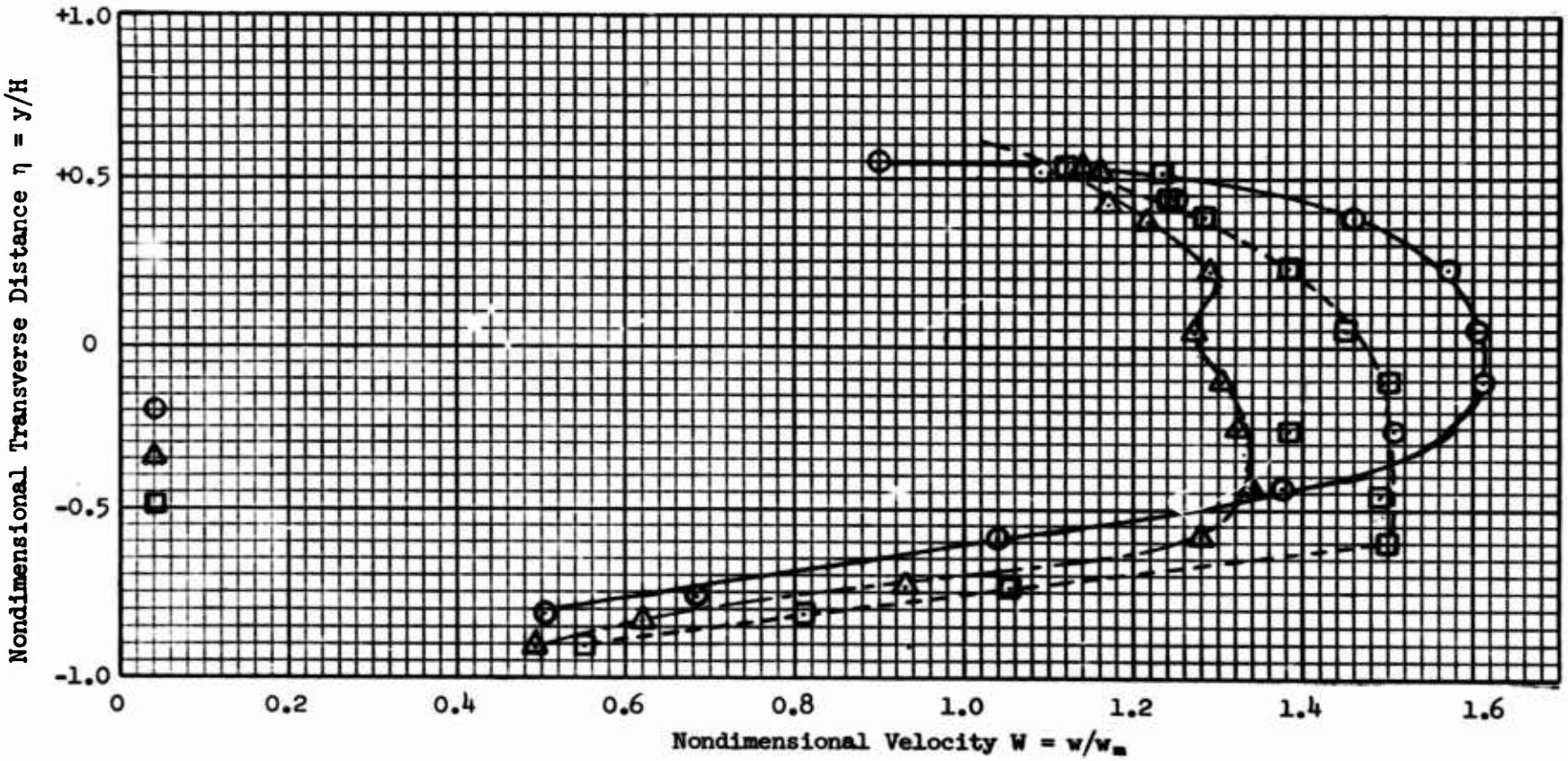

Fig. 25 - Nondimensional velocity profiles for Reynolds number of 265, for various charge numbers

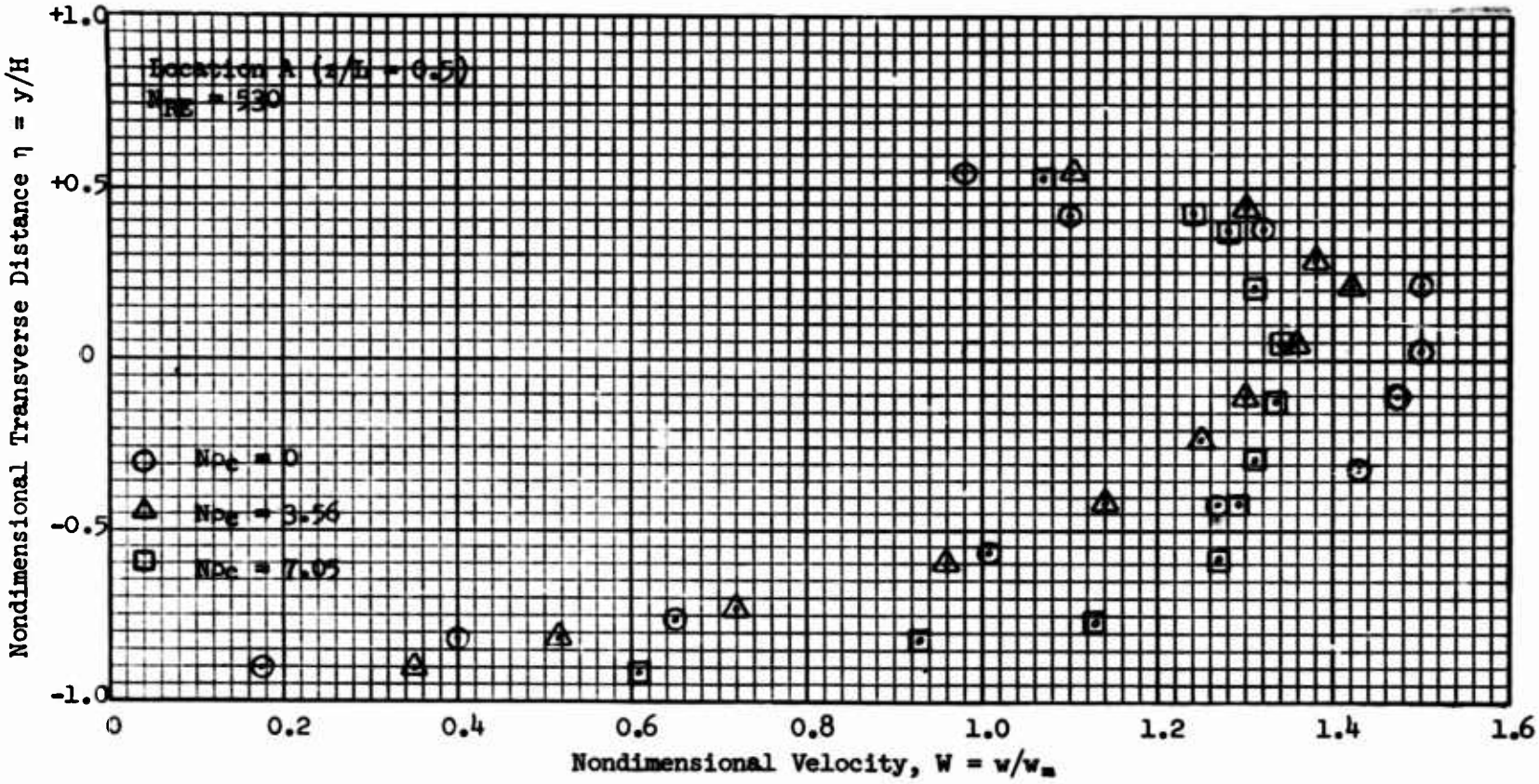

Fig. 26 - Nondimensional velocity profiles for Reynolds number of 540, for various charge numbers

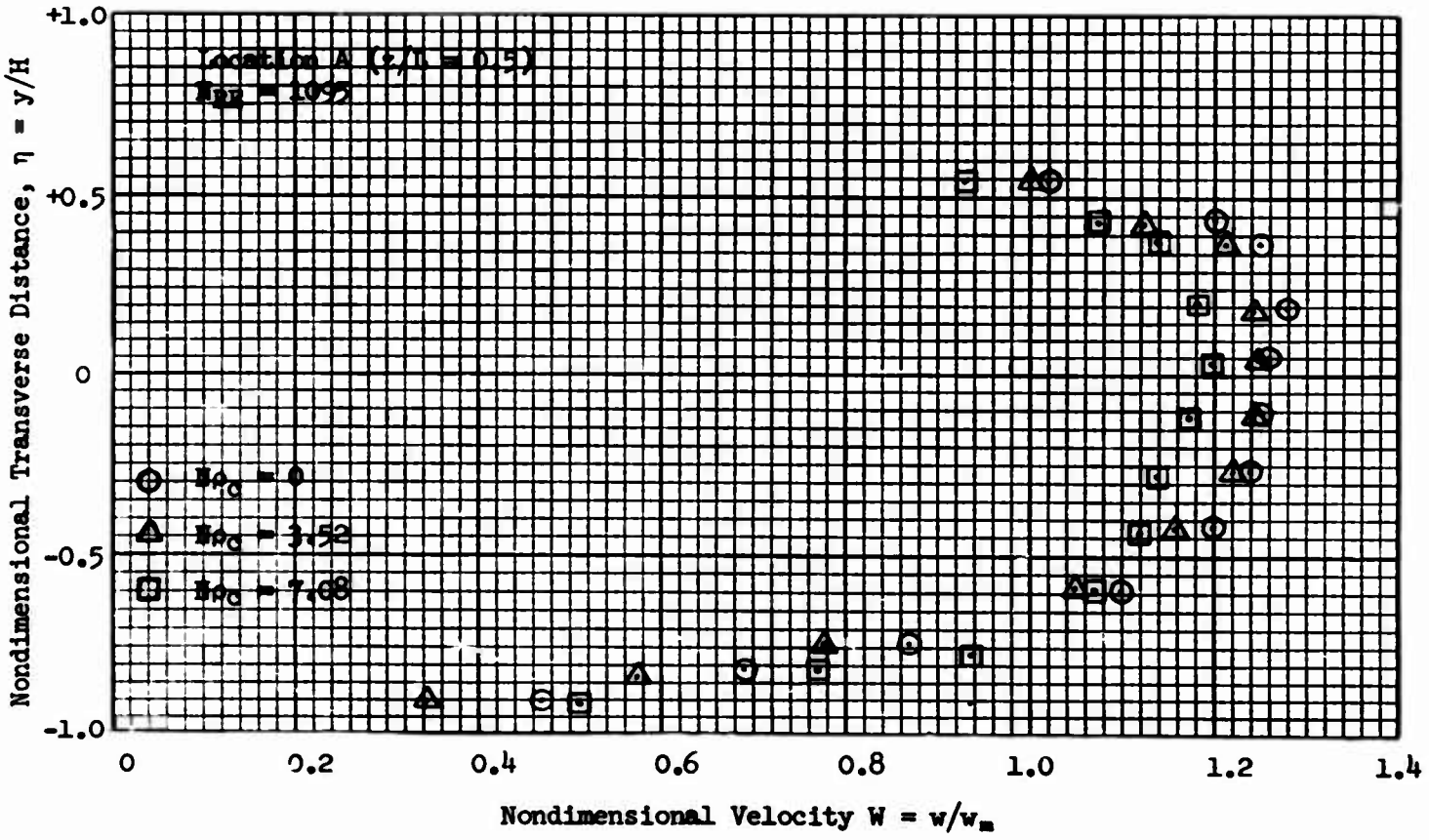

Fig. 27 - Nondimensional velocity profiles for Reynolds number of 1095, for various charge numbers

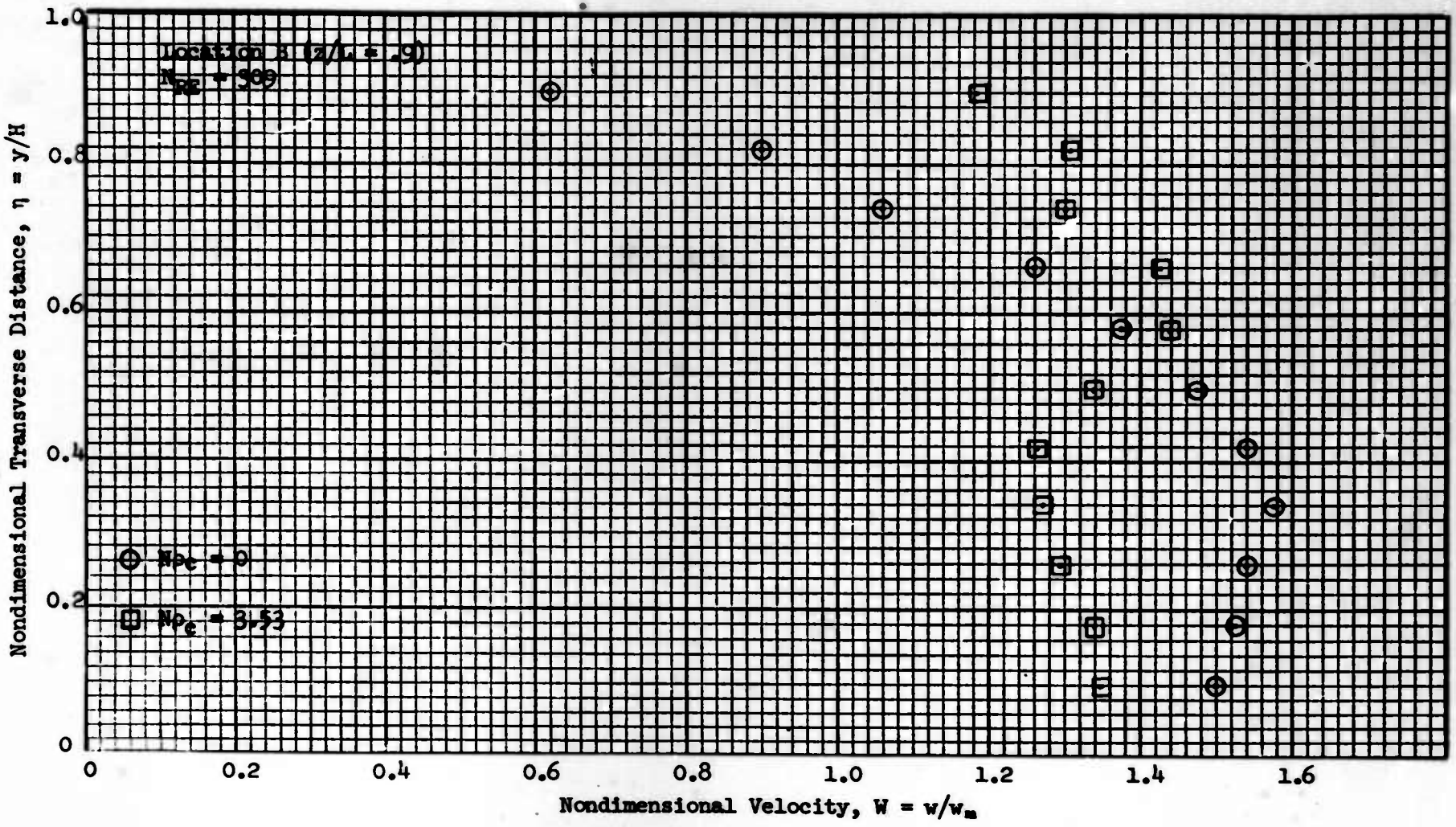

Fig. 28 - Nondimensional velocity profile at location B

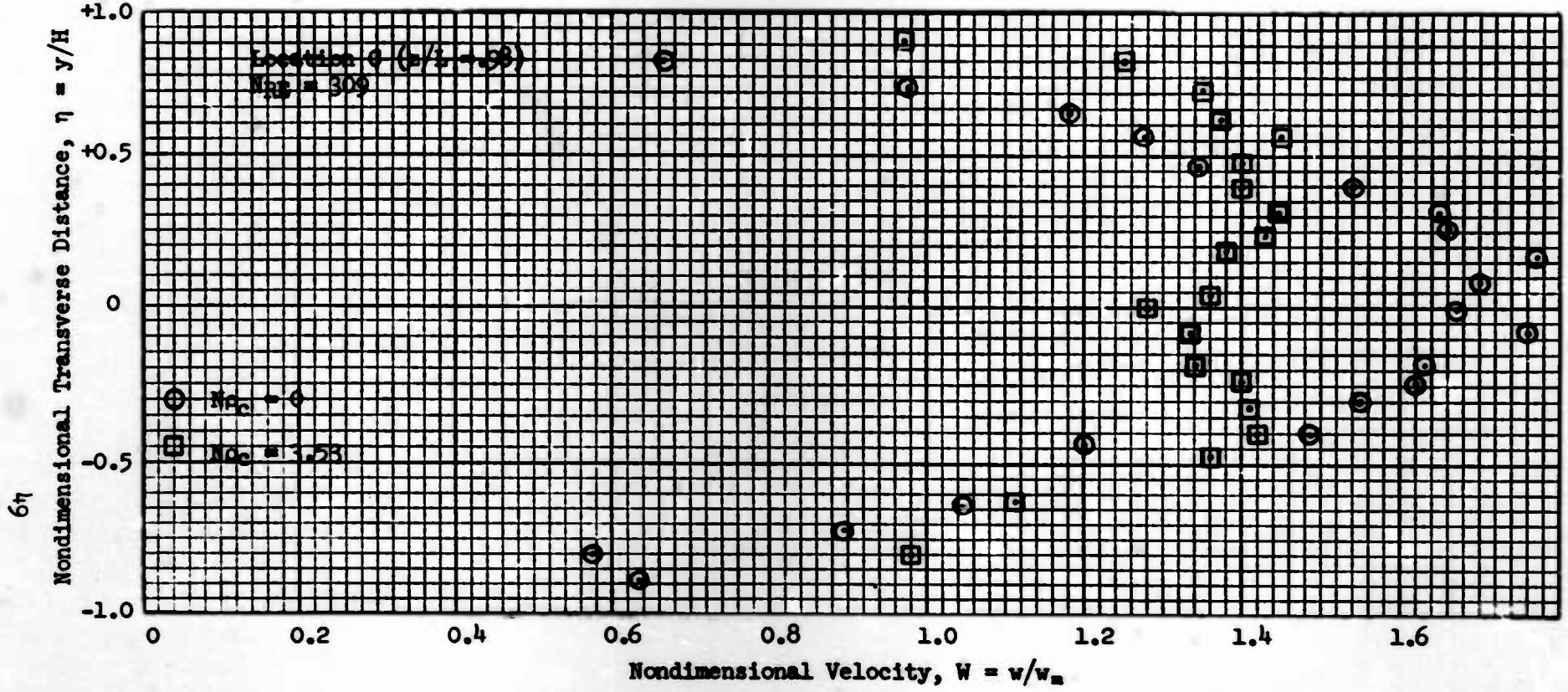

Fig. 29 - Nondimensional velocity profile at location C

$$\frac{\partial E_z}{\partial y} = \frac{\partial E_y}{\partial z}$$

As a limiting case, the approximate theory indicates

$$E_z = - w/K \tag{23}$$

Assuming K is constant, then

$$- \frac{1}{K} \frac{\partial w}{\partial y} = \frac{\partial E_y}{\partial z} \quad . \tag{55}$$

Since fully established flow is considered, $w \neq f(z)$, hence

$$w = f(y) \text{ alone} \tag{56}$$

and

$$\frac{\partial w}{\partial y} = - f_1(y) \quad . \tag{57}$$

Thus

$$\int_{z=z_1}^{z_2} dEy = \frac{1}{K} \int_{z_1}^{z_2} f_1(y) dz \tag{58}$$

$$Ey_{z_2} - Ey_{z_1} = \frac{f_1(y)}{K} (z_2 - z_1) \quad . \tag{59}$$

This above analysis indicates that unless w is a constant value across the channel, we can expect that a variation in E_y will occur along the axis of the channel. If one examines the characteristics of a corona discharge, see for example Fig. 9, it is readily apparent that the discharge is highly sensitive to changes in voltage. In the cirtical discharge region, a small change in voltage will lead to a large change in current. Since the internal field in the transverse or y direction is related closely to the voltage, it can be expected that if changes in the transverse field, E_y, occur along the channel, then changes in the local transverse current, J_y, should result.

From the foregoing analysis, one should expect to see an approximately linear change in E_y along the channel. If this occurs, then one would expect to find that the corona currents increased along the length of the channel. Under such conditions for a very long channel, it could be expected that the air flowing along the channel would induce very high local E_y fields at the end of the pipe, perhaps sufficient to lead to breakdown. Since a variation of E_y along the pipe was predicted from the analysis, it was decided to conduct a test to determine the variation of current density along the channel.

In the initial tests, the grounded channel walls were constructed of single pieces, and measurement of local current density was impossible. The flow channel was later modified by covering one grounded wall with an insulating covering and painting it with transverse strips of conductive silver paint, each strip being separated from the adjacent one by a thin unpainted area approximately 1/32-inch wide. The current to each strip divided by the area of that strip then gives the local current density at the location of that strip. (See Fig. 30) These modifications were made to determine the extent to which ion density is affected by the air flow.

Figure 31 shows the current density profile for zero, 265, and 860 Reynolds number. The curves show only a slight shift in shape, toward a higher density downstream with air flow, as expected. The curve for zero air flow is not flat because slight changes in Geometry along the duct due to wire sag and duct alinement greatly affect local current density. The isolated points on Fig. 31, showing low values of current density, are caused by the effect of nylon filaments stretched across the duct to support the corona wires and eliminate wire sag.

Figure 32 shows the average current density for an area of duct wall in the upstream half of the duct and an area of wall in the downstream half of the duct, as a function of Reynolds number. It is seen that the air flow acts to force a higher current density downstream and a lower current density upstream. The amount of change depends on the Reynolds number below about 400, and is independent of the Reynolds number above 400. These curves indicate that an ion-fluid coupling does exist and suggest that the postulated flow induced body force may possibly exist.

Flow Visualization Attempts

Smoke was injected into the channel through the total pressure probes to obtain a visualization of the flow field. (The side walls were transparent Plexiglas). Although smoke particles are inherently charged, their mass is large compared to an ion, and therefore, they would drift to the electrodes much more slowly than the ion drift, and hopefully the smoke particle motion would be affected by the local fluid motion in the duct.

With no ion current, the smoke stream provided a clearly defined visualization of the streamlines, but upon the onset of ion current, the smoke pattern was rapidly diffused, mixed with the air, and precipitated, resembling a turbulent motion in appearance. Consequently, no characteristic flow pattern was discernable with the smoke studies.

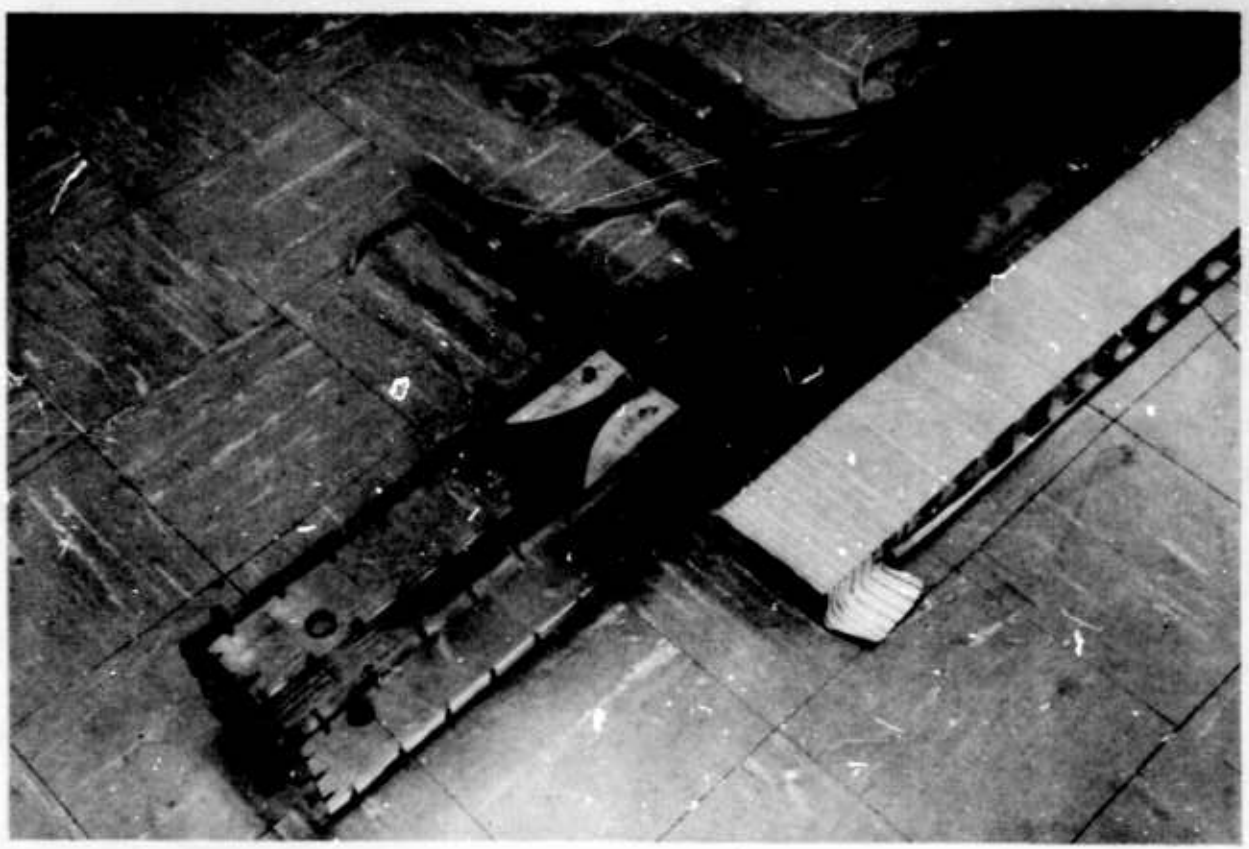

Fig. 30 - Photograph of the flow channel with one wall removed, showing the segmented electrode

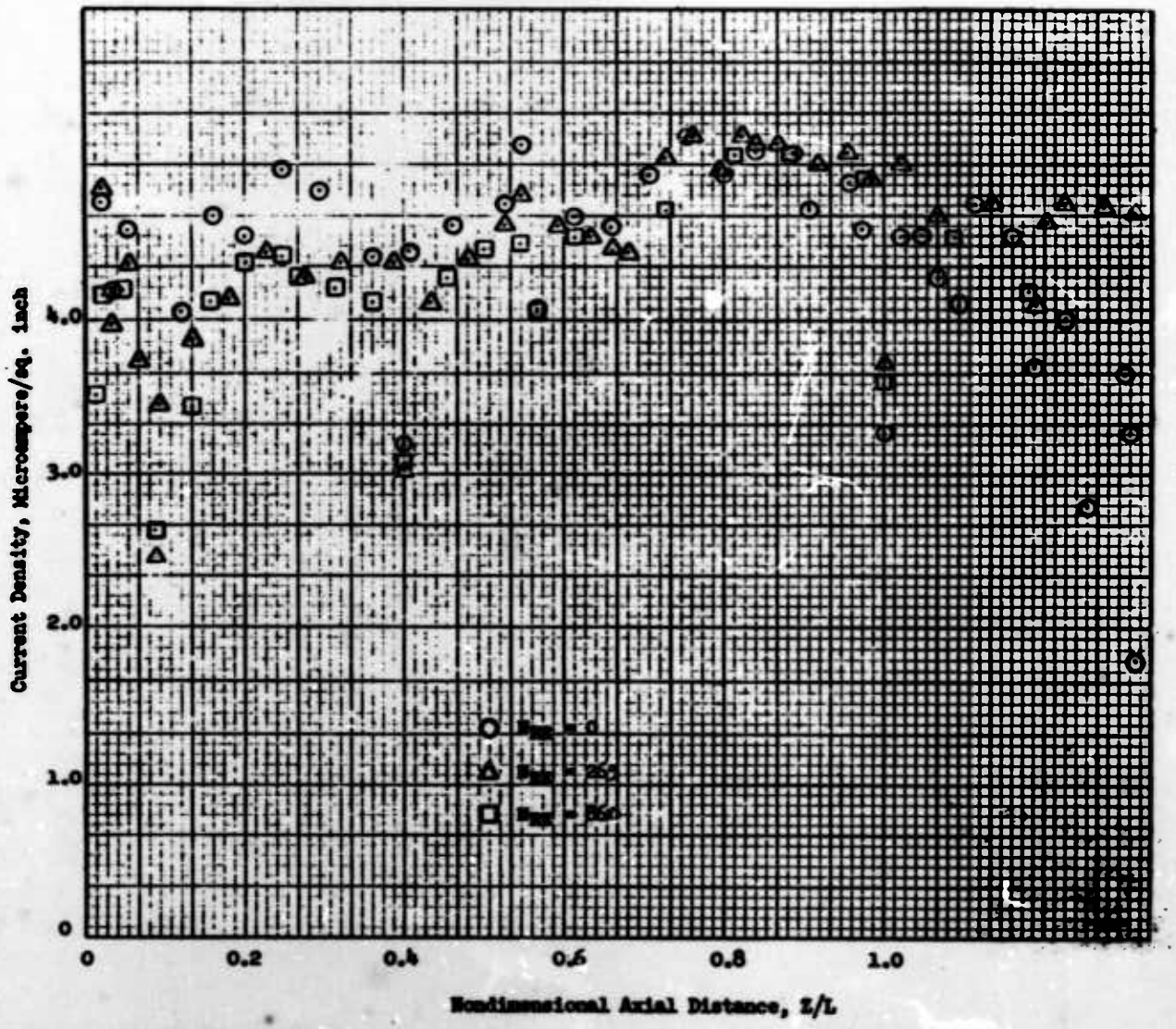

Fig. 31 - Current density measured at lower wall vs. axial distance with Reynolds number as parameter

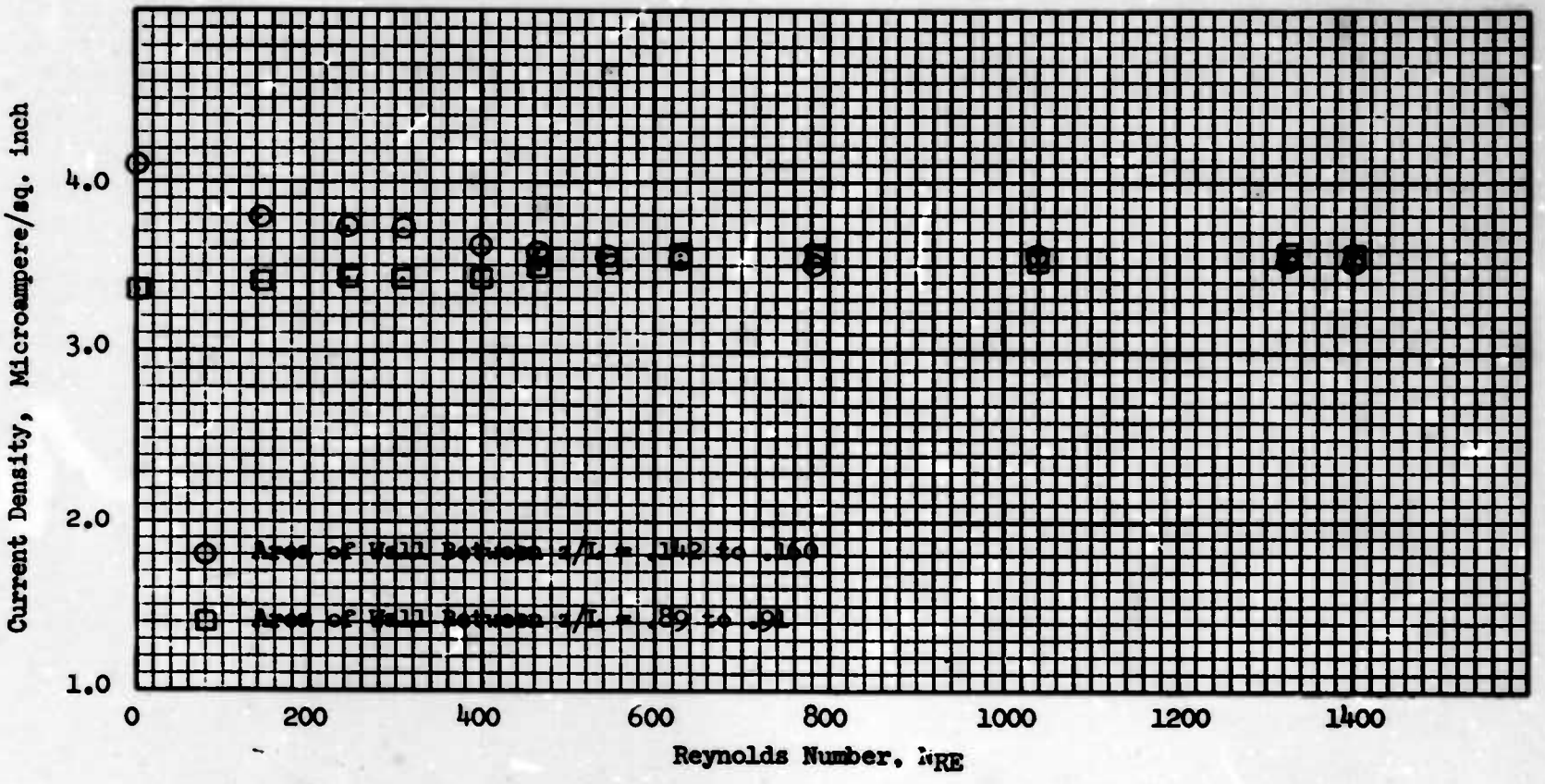

Fig. 32 - Current density at lower wall versus Reynolds number, for two different values of axial distance Z

Supplementary Tests

Effect of Fringing Field

Although the static pressure drop along the flow direction was measured as a straight line, indicating that the ion effect was continuously active throughout the duct length and was not an end effect, the following test was performed to determine the influence of the electrical end effect, or "fringing field." Several 2-inch-wide transverse conducting strips at different locations along the length were disconnected from ground and left "floating" with no current. Air passing completely through the duct then would have the effect of passing through six channels in series, as far as the electric field on the lower half of the duct is concerned. The upper grounded wall was not provided with separate conducting strips and hence was at ground potential completely.

With the above arrangement, the discontinuous electric field had practically no effect on the friction factor, (Fig 33) and hence it was concluded that the ion coupling effect is definitely not a surface or "end" effect.

Effect of Number of Wires

Throughout all of the test work, there were 10 corona wires, spaced at 1/2-inch intervals across the 5-inch width of the duct. To determine the importance of the number of ion producing sites, one experimental measurement of friction factor was done with only five wires, spaced at one-inch intervals, impressed with voltage. The other five wires were left in place, but disconnected. Figure 34 shows the pressure drop along the duct compared with a test using ten wires, both tests being at the same total current. The corresponding friction factor for the five wire run was 21% larger than the ten-wire case. The difference is attributed to the fact that with one-inch wire spacing the ratio of wire spacing to half height of the duct becomes too large to maintain geometrical similarity with the ten-wire case.

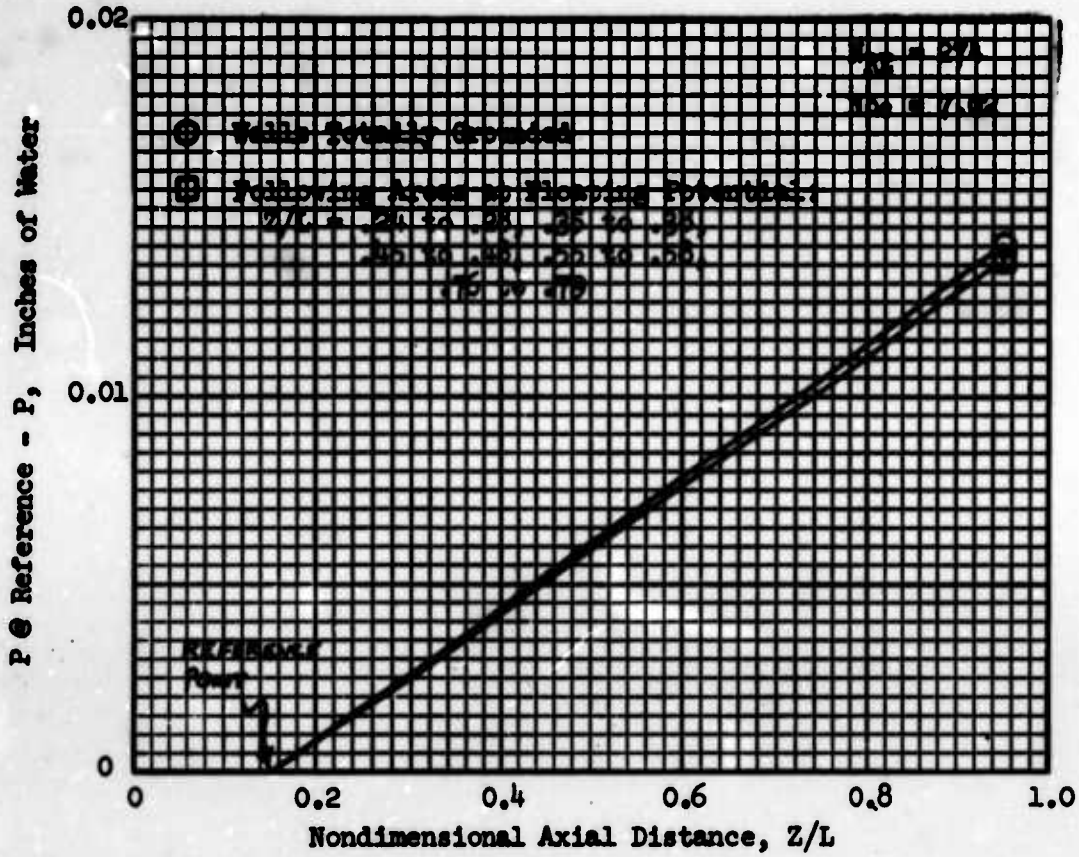

Fig. 33 - Static pressure on upper wall versus axial distance Z/L showing effect of discontinuous electric field along the duct

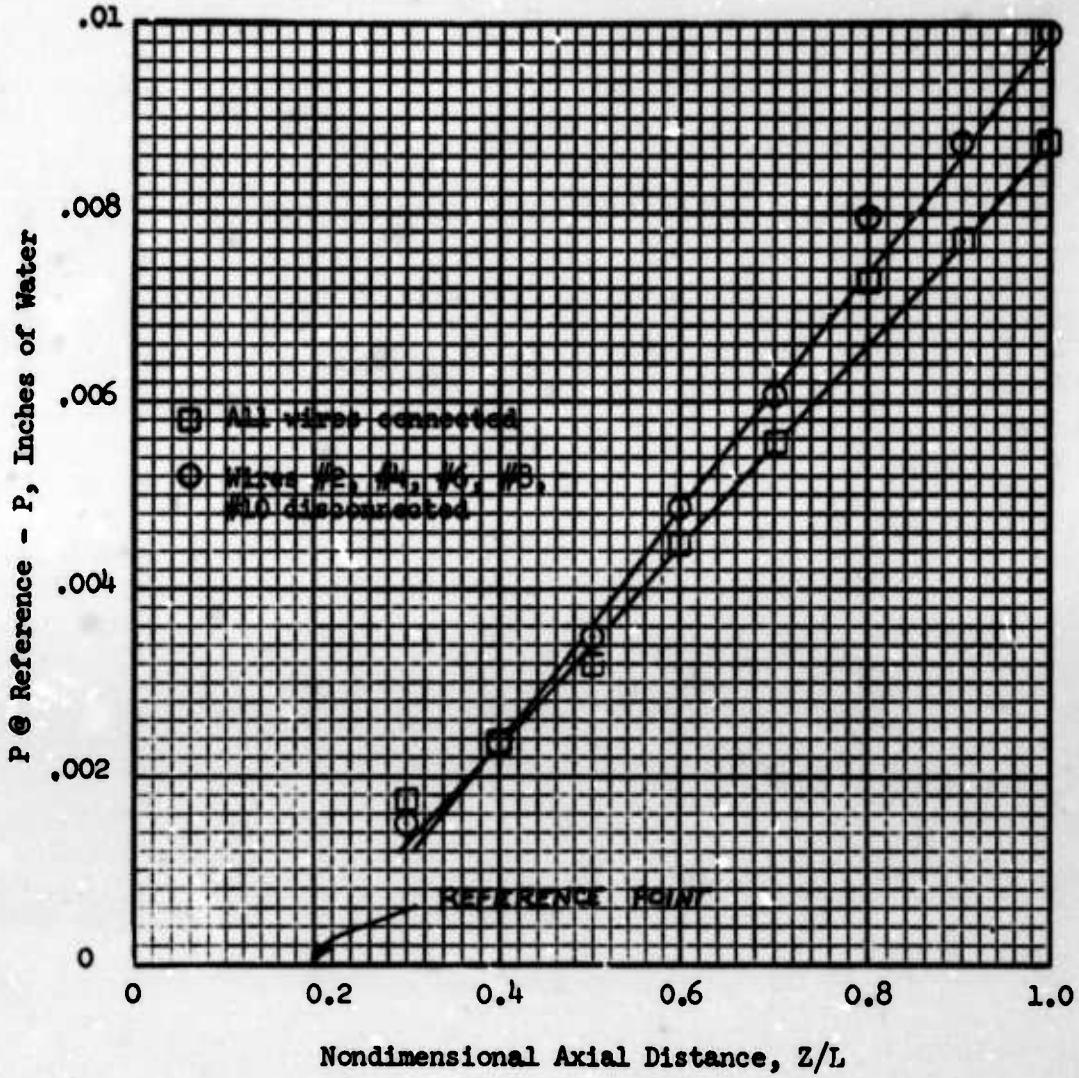

Fig. 34 - Static pressure on upper wall versus axial distance Z showing the effect of number of corona wires

SECTION IV

CONCLUSIONS AND RECOMMENDATIONS

The effects of transverse ion flow on the flow of air in a rectangular duct were shown to display the same trends as found earlier[3] in experiments on a circular pipe. Friction factors were significantly increased, velocity distributions distorted, and a useful correlating parameter, the charge number, could be defined.

Experimentally, it was found that the laminar flow friction factor was an almost linear function of the nondimensional charge number, $N\rho_c$, as predicted by one of the approximate solutions. The data was well represented by the relation

$$f = \frac{9.2}{N_{RE}} (1 + 0.13\, N\rho_c)$$

up to a charge number of 8.2, which was the greatest charge number investigated.

The transverse ion flow was found to generate an electric pressure gradient transverse to the air flow which agreed closely with the theoretical expression for a planar ion source,

$$\frac{\partial p}{\partial y} = \frac{J_y}{K} \quad ,$$

near the channel walls. Near the midplane of the channel where the corona wires were located, the above expression was not applicable because of the individual effect of the wires which deviated from the ideal planar ion source.

Velocity distributions across the flow channel were significantly distorted by the ion current. Typically, the centerline velocity was decreased and the velocity gradient at the walls increased.

Local transverse ion current density at the channel wall was measured and found to be dependent on the air velocity within the channel. The effect of the air flow was to cause an increase in current density in downstream parts of the channel and a decrease in upstream parts. At sufficiently high velocity no further change in current density was noted.

It is recommended that further work be done to determine the type of possible ion-fluid coupling mechanisms and the extent to which they are active in specific fluid-flow configurations. Included among the various possible ion-fluid coupling mechanisms we find (1) the direct generation of electric wind, causing mass motion along the direction of the electric field,[8] (2) the generation of secondary flows induced by electric body forces, (3) the modification of the transport properties of the fluid medium caused by ion motion,

(4) the generation of flow-induced electric body forces, which is treated in this report and elsewhere,[2,3,9] the destabilization of a fluid interface when two fluids or phases are present.[10,11] Such mechanisms are distinct from effects caused by a non-uniform electric field in fluids with a dipole moment.[12]

Experimental and theoretical work is in progress on the study of flow instabilities caused by electric body forces, item (2) above, which has been discussed in the literature as formation of toroidal cells[13] or longitudinal roll cells,[13,14] and its analogy with magnetic fields.[15] Such secondary flows have analogies in classical fluid mechanics where the destabilizing body forces are caused by centrifugal force fields or gravitation force fields.[16]

It is anticipated that further experimental work will include the application of electrostatic probes to the direct measurement of ion density and field gradient within a moving fluid, and the development of flow visualization techniques suitable for use in electric fields.

REFERENCES

1. Velkoff, H. R., "An Exploratory Investigation of the Effects of Ionization on the Flow and Heat Transfer in a Dense Gas," ASD-TDR-63-842. Aero Propulsion Laboratory, ASD, Air Force Systems Command, Wright-Patterson Air Force Base, Ohio, 1963.

2. Velkoff, H. R., "The Effects of Ionization on the Flow and Heat Transfer of a Dense Gase in a Transverse Electrical Field," Proceedings of the 1964 Heat Transfer and Fluid Mechanics Institute, Stanford University Press, Stanford, California, 1964.

3. Velkoff, H. R., "An Analysis of the Effect of Ionization on the Laminar Flow of a Dense Gas in a Channel," RTD-TDR-63-4009, Aero Propulsion Laboratory, Air Force Systems Command, Wright-Patterson Air Force Base, Ohio, 1963.

4. Steutzer, O. M., "Ion Drag Pressure Generation," J. Appl. Phys., Vol. 30, 1959, p. 984.

5. Cobine, J. D., Gaseous Conductors, Dover Publications Inc., New York, New York, 1958.

6. Holt and Haskell, Plasma Dynamics, p. 162, Macmillan, New York, New York, 1965.

7. Present, Kinetic Theory of Gases, p. 55, McGraw-Hill, New York, New York, 1958.

8. Velkoff, H. R., "Electrofluidmechanics: Investigation of the Effects of Electrostatic Fields on Heat Transfer and Boundary Layers," Propulsion Laboratory, ASD, Air Force Systems Command, Wright-Patterson Air Force Base, Ohio, Sept., 1962.

9. Kopylov, G. N. "Laminar Flow of a Charged Liquid through a Plannar Tube under the Influence of an External Electrostatic Field," Soviet Physics-Technical Physics, Vol. 8, No. 11, May, 1964.

10. Melcher, J. R., Field-Coupled Surface Waves, Massachusetts Institute of Technology Press, Cambridge, Mass., 1963.

11. Velkoff, H. R., Miller, J. H., "The Effect of an Electrostatic Field on the Condensation of Vapor," Air Force Aero Propulsion Laboratory, Air Force Systems Command, Wright-Patterson Air Force Base, Ohio, February, 1964.

12. Schmidt, E., Leidenfrost, W., "Der Einfluss Elektrischer Felder Auf Den Warme Transport in Flussigen Elektrischen Nichtleitern" Furschung Auf Dem Gebiete Des Ingenieurwesens, No.3, 1953.

13. Malkus, W. V., Veronis, G. "Surface Electroconnection," Phys. Fluids, Vol. 4, No. 1, p. 13-23, January, 1961.

14. Benion, D. N. et al., "Transport Processes in Electrode Systems," March, 1965, AD 621842, ARPA No. 220-61, U.S. Army Electronic Laboratories Contract No. DA 36-039 SC-89153, Fort Monmouth, New Jersey.

15. Yih, Chia-Shun, "Ring Vortices Generated Electromagnetically," J. Fluid Mech. Vol. 3, p. 436, 1959.

16. Chandrasekhar, S., Hydrodynamic and Hydromagnetic Stability, Clarendon Press, Oxford, England, 1961.

SECTION VI - APPENDICES

APPENDIX I

HYDRODYNAMIC AND ELECTRODYNAMIC EQUATIONS

Momentum Equation

y direction

$$\rho \frac{Du}{Dt} = - \frac{\partial p}{\partial y} + \mu \nabla^2 u + \frac{\mu}{3} \frac{\partial}{\partial y}\left(\frac{\partial u}{\partial y} + \frac{\partial w}{\partial z} \right) + F_y \qquad (60)$$

z direction

$$\rho \frac{Dw}{Dt} = - \frac{\partial p}{\partial z} + \mu \nabla^2 w + \frac{\mu}{3} \frac{\partial}{\partial z}\left(\frac{\partial u}{\partial y} + \frac{\partial w}{\partial z} \right) + F_z \qquad (61)$$

Mass Continuity

$$\frac{\partial \rho}{\partial t} + \frac{\partial (\rho u)}{\partial y} + \frac{\partial (\rho w)}{\partial z} = 0 \qquad (62)$$

Charge Continuity

$$\frac{\partial \rho_c}{\partial t} + \frac{\partial J_y}{\partial y} + \frac{\partial J_z}{\partial z} = 0 \qquad (63)$$

Body Force

$$F_y = \rho_c E_y + \mu_e (\vec{J} \times \vec{H})_y + \frac{\epsilon}{2} \rho \nabla \left[\vec{E} \cdot \vec{E} \left(\frac{\partial \epsilon}{\partial \rho} \right)_T \right]_y - \frac{\epsilon}{2} \vec{E} \cdot \vec{E} \left(\frac{\partial \epsilon}{\partial T} \right)_\rho \frac{\partial T}{\partial y} \qquad (64)$$

$$F_z = \rho_c E_z + \mu_e (\vec{J} \times \vec{H})_z + \frac{\epsilon}{2} \rho \nabla \left[\vec{E} \cdot \vec{E} \left(\frac{\partial \epsilon}{\partial \rho} \right)_T \right]_z - \frac{\epsilon}{2} \vec{E} \cdot \vec{E} \left(\frac{\partial \epsilon}{\partial T} \right)_\rho \left(\frac{\partial T}{\partial z} \right) \qquad (65)$$

Maxwell's Equations

$$\vec{\nabla} \times \vec{H} = \vec{J} + \frac{\partial (\epsilon \vec{E})}{\partial t} \qquad (66)$$

$$\vec{\nabla} \times \vec{E} = - \frac{\partial (\mu_e \vec{H})}{\partial t} \qquad (67)$$

$$\vec{\nabla} \cdot \vec{H} = 0 \tag{68}$$

$$\vec{\nabla} \cdot \vec{E} = \frac{\rho_c}{\epsilon} \tag{69}$$

Equation of State

$$p = \rho RT \tag{70}$$

Ohm's Law

$$\vec{J} = \sigma[\vec{E} + \mu_e(\vec{v} \times \vec{H})] + \rho_c K\vec{E} - D\,\vec{\nabla}\,\rho_c \tag{71}$$

where a subscript y or z signifies the component of that quantity in the y or z direction, respectively.

APPENDIX II

APPROXIMATE ANALYSIS SATISFYING THE IRROTATIONAL ELECTRIC FIELD CONDITION

By formulating the electro-fluid dynamic equations as a one-dimensional problem, it was shown previously (Eq. (9)) that Eq. (7), which is the condition that curl E = 0, leads to the result that the velocity is constant, and therefore zero everywhere. The analysis was continued, but for a finite velocity the approximate theory violates the electrodynamic Eq. (7), the condition of an irrotational voltage field.

In the following analysis, Eq. (7) is alway satisfied, i.e., curl E = 0, and the field is a potential field, but it results in a violation of Eq. (16), which is the relation governing the electric field distortion by space charges.

From Eq. (5)

$$E_z = -\frac{w}{K} \quad . \tag{23}$$

Substituting in Eq. (7)

$$\frac{\partial E_y}{\partial z} + \frac{1}{K}\frac{\partial w}{\partial y} = 0 \quad . \tag{72}$$

Since w is a function of y only, E_y must be linear in z. Therefore, we take

$$E_y = \left[1 + \beta \frac{z}{H}\right] f(y) \tag{73}$$

where β is a constant and f(y) is a function of y.

For the y dependency of E_y, we take the relation of Eq. (19), based on space charge limited current and zero velocity. Then

$$E_y = \left[1 + \beta \frac{z}{H}\right]\left[\frac{2J_y y}{K\epsilon}\right]^{1/3} \quad . \tag{74}$$

Substituting into Eq. (72) and integrating,

$$w = \frac{2}{3}\,\frac{\beta}{H}\left[\frac{2J_y K}{\epsilon}\right]^{1/3}\left[H^{3/2} - y^{3/2}\right] \tag{75}$$

which is an expression for the velocity distribution obtained without consideration of the fluid momentum (Eq. (10)). If we put Eq. (75) into Eq. (23) and Eq. (74) into Eq. (12)), it is possible to obtain an expression for the electric body force term, $\rho_c E_z$.

$$\rho_c E_z = \frac{2}{3} \frac{\beta}{H} \frac{J_y}{K y^{1/2}} \left[H^{3/2} - y^{3/2} \right] . \tag{76}$$

Using this force term in Eq. (10) and integrating Eq. (10) twice,

$$w = \frac{\beta J_y}{9 H \mu K} \left[y^3 - 8 H^{3/2} y^{3/2} + 7 H^3 \right] + \frac{1}{2\mu} \frac{\partial p}{\partial t} \left[y^2 - H^2 \right] \tag{77}$$

where the first term is the electric-induced term and the second term is the classical-parabolic term.

Calculating the mean velocity from Eq. (77), the friction factor can be calculated.

$$f = \frac{6}{N_{RE}} \left[1 - \frac{27}{80} \beta \, N\rho_c \, N_\alpha \right] \tag{78}$$

where

$$Nd = \text{drift number} = \left[\frac{8 J_y K H}{9 E W_m^2} \right]^{1/2} = \frac{\text{drift velocity}}{\text{mean velocity}} .$$

If Eq. (74) and Eq. (12) are combined into Eq. (16), a contradiction results; therefore, the above analysis does not satisfy the condition of Eq. (16).

The above analysis indicates that the friction factor, f, varies with J_y and that fN_{RE} varies with N_{RE}^{-1}. It was verified experimentally, however, that f varies with $J_y^{1/2}$ and fN_{RE} is constant in laminar flow, and, therefore, the above analysis is not a realistic model of the ion-fluid coupling.

APPENDIX III

EFFECT OF NEARBY SURFACES ON CORONA

In the early channel flow tests, corona wires were stretched along a plastic surface (Plexiglas) which formed one wall of the duct. It was found that the corona current characteristic was non-uniform and frequently not repeatable. Since it was thought that small variations in the distance between the corona wires and the dielectric surface might be important in the corona current-voltage characteristic, an apparatus was constructed to determine the magnitude of the effect of a nearby dielectric surface to a corona discharge. The apparatus, shown below, maintained a fixed distance between the plane grounded electrode and the corona wire while the distance from the corona wire to a Plexiglas surface could be varied by a screw adjustment.

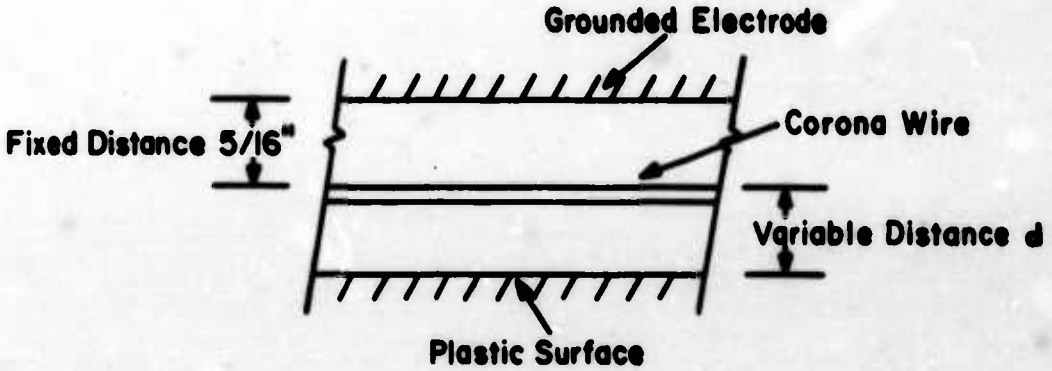

A 0.010-inch wide x 1/32-inch-deep slot was cut in the Plexiglas surface to enable the surface to move beyond the 0.004-inch-diameter wire. Figure 35 shows the effect of d, the distance from the wire to the plastic surface. It is seen that for small values of d the current-voltage curves become steeper, and sparking from the wires to the ground electrode occurs at a lower voltage. For d=0, the result was that no corona current occurred at all voltages up to the sparking voltage. Therefore, the effect of the plastic surface was very critical to the corona characteristic for small values of d.

It was desired to also determine the effect of an air flow over a corona discharge while being affected by the proximity of a dielectric surface. For this purpose a needle utilized as a corona point was maintained concentric within a hole in a nylon spool. The spool could be raised or lowered to allow various lengths of the needle to protrude beyond the hole in the spool, as shown below. The distance from the grounded plane electrode to the needle at positive voltage was held constant while the

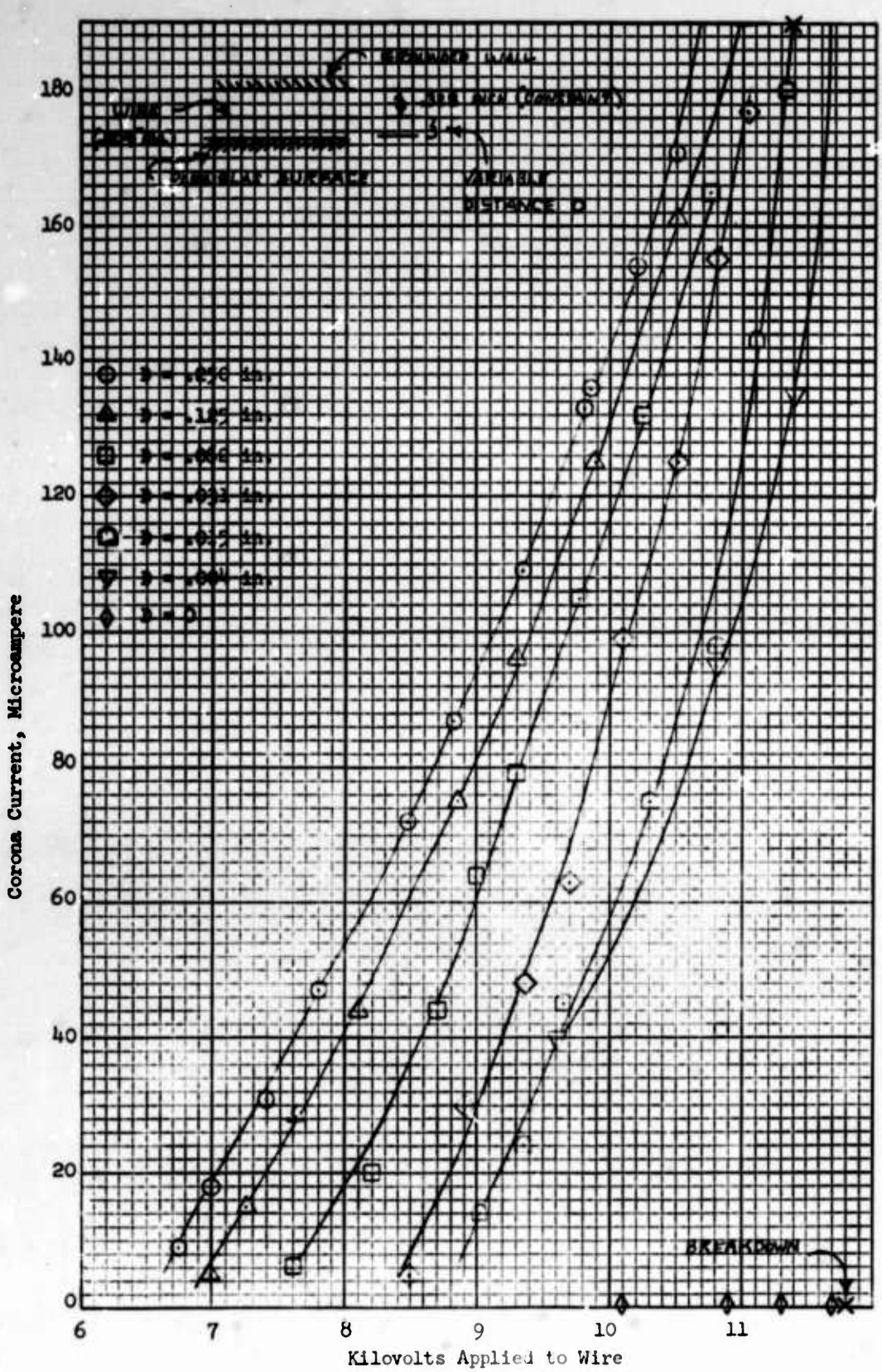

Fig. 35 - Corona current versus voltage applied, showing the effect of a nearby surface

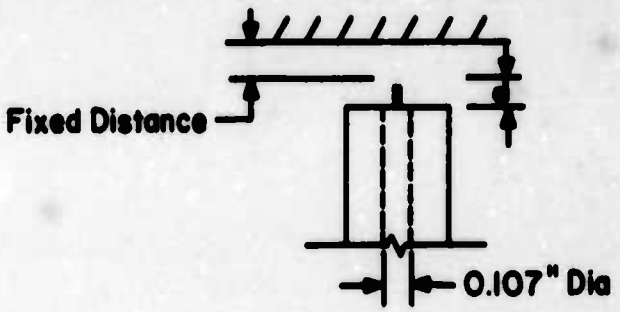

distance d could be varied and the air flow through the hole in the spool could be metered. Figure 36 shows the effect of distance d on the (ampere) voltage characteristic, which shows that for the needle tip closer to the nylon spool the current-voltage curve is steeper and that sparking occurs at a lower voltage in agreement with the previous results on the wire.

Figure 37 shows the effect on the corona characteristic of air flow through the hole in the spool. As indicated on the figure, at the end of the test of Fig. 37, the current at zero air flow was measured again and found to be 8.5μ amp where it was 13.9μ amp at the beginning of the test. This difficulty of a changing corona characteristic of the needle point is a result of the wearing away of the needle tip with current, which changes the radius of curvature of the needle tip. A change in curvature then changes the field strength at the needle tip and changes the current-voltage characteristic.

Because of the effect on the needle tip, repeatable results were not obtainable. However, it was found that there is an effect of the air flow on the corona current. Figure 37 shows that the current increased with higher velocity air flows, porbably resulting from a flow-induced change in the space charge around the needle. It is to be noted, however, that the air velocities of Fig. 37 go up to 500 feet per second, while the flow velocities used in subsequent channel flow tests were about 1 to 10 feet per second. For less then 10 feet per velocity, the slope of the data points in Fig. 37 would indicate a negligible charge in corona current. Indeed, Fig. 6 shows no effect of flow on the corona characteristic for Reynolds numbers of up to 1270, corresponding to a flow velocity of up to 10 feet per second.

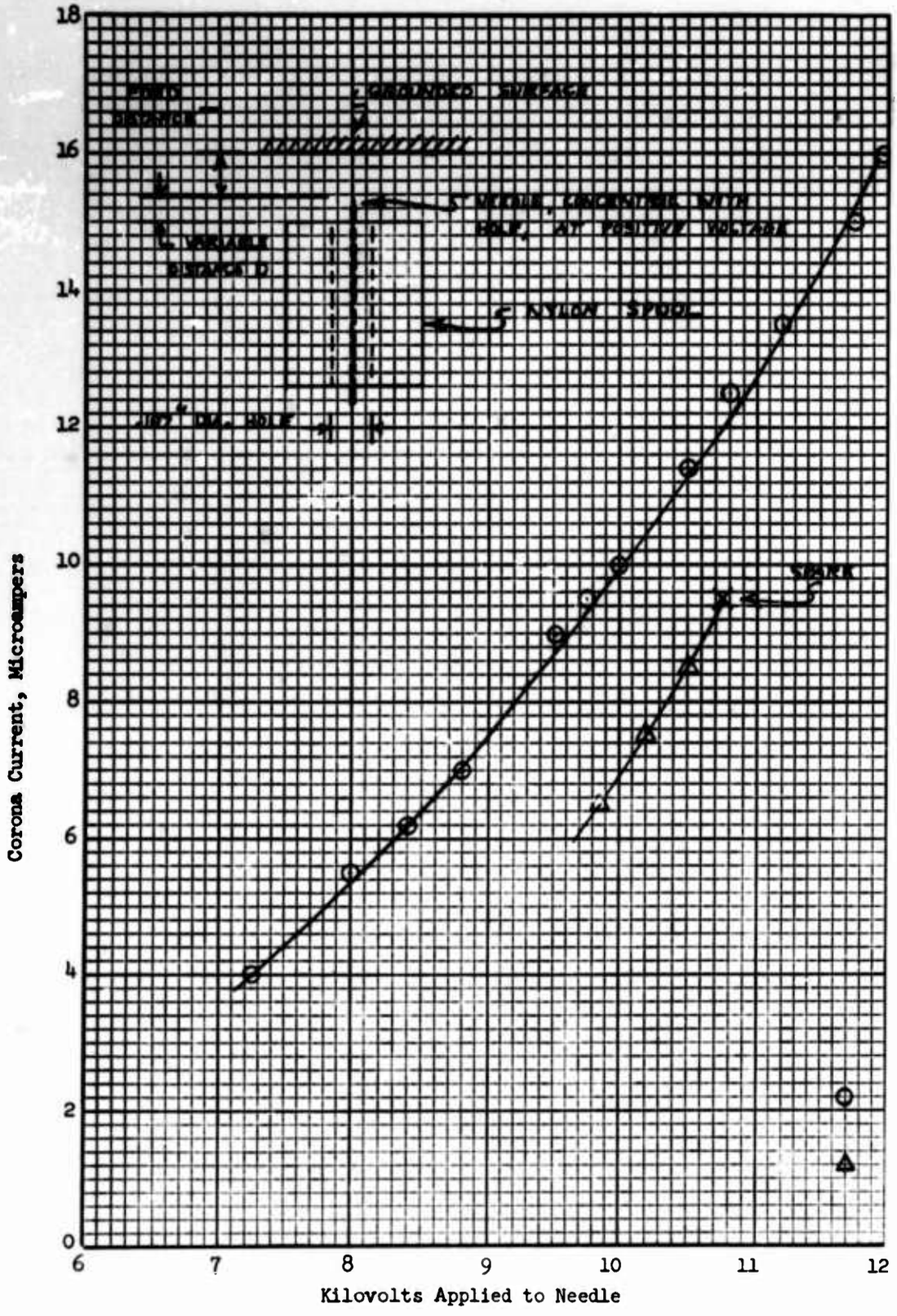

Fig. 36 - Corona current versus voltage applied to a needle point, showing the effect of geometry

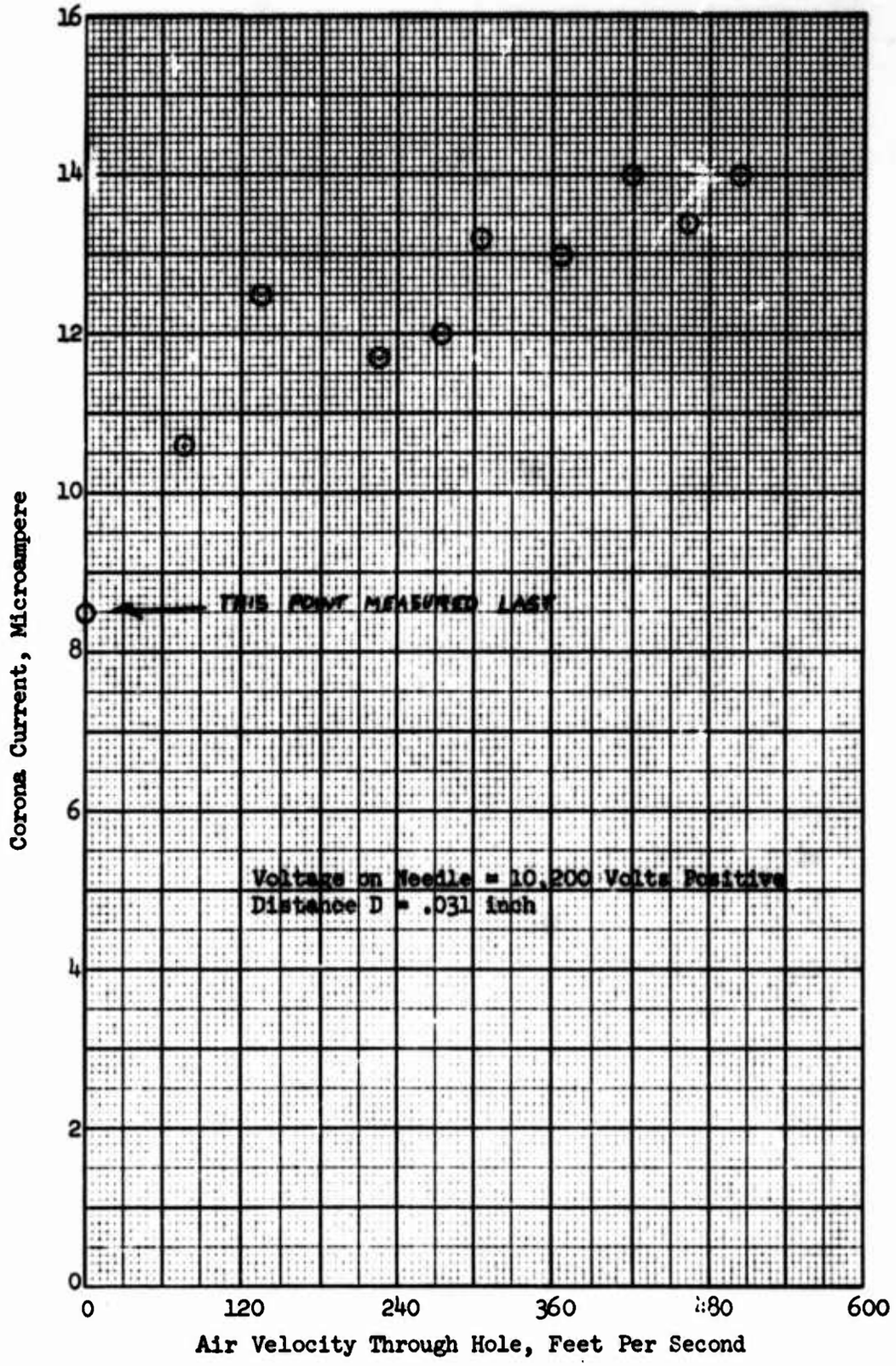

Fig. 37 - Corona current versus voltage applied to a needle point, showing the effect of a superimposed air stream

Unclassified
Security Classification

DOCUMENT CONTROL DATA - R&D
(Security classification of title, body of abstract and indexing annotation must be entered when the overall report is classified)

1. ORIGINATING ACTIVITY (Corporate author) Ohio State University Research Foundation	2a. REPORT SECURITY CLASSIFICATION Unclassified 2b. GROUP

3. REPORT TITLE

The Effect of Transverse Ion Current on the Flow of Air in a Flat Duct.

4. DESCRIPTIVE NOTES (Type of report and inclusive dates)

Technical Report February, 1967

5. AUTHOR(S) (Last name, first name, initial)

Pejack, Edwin R.
Velkoff, Henry R.

6. REPORT DATE	7a. TOTAL NO. OF PAGES	7b. NO. OF REFS
February, 1967	79	16

8a. CONTRACT OR GRANT NO. DA-31-124-ARO-D-246	9a. ORIGINATOR'S REPORT NUMBER(S)
b. PROJECT NO. 20010501B700	
c. 1D12140A142	9b. OTHER REPORT NO(S) (Any other numbers that may be assigned this report)
d.	

10. AVAILABILITY/LIMITATION NOTICES

Distribution of this document is unlimited.

11. SUPPLEMENTARY NOTES	12. SPONSORING MILITARY ACTIVITY
	U.S. Army Research Office - Durham Box CM, Duke Station Durham, North Carolina

13. ABSTRACT

Friction factors, velocity distributions, pressure gradients, and density measurements were made on a 5/8-inch x 5-inch rectangular flow channel with air flow. A plane of corona wires along the midplane of the channel was the source of ions which drifted across the air flow to the electrically grounded walls of the channel. Experimental data were collected to determine the influence of the ion flow on the air flow and the extent of the ion-fluid coupling.

The electrodynamic and hydrodynamic equations were set up and several approximate solutions were obtained based on the postulation of a flow induced body force and the assumption of fully established, one-dimensional flow. The magnitude of the ion effects was found to be significantly dependent on the ion density distribution within the flow channel.

DD FORM 1 JAN 64 1473

Unclassified
Security Classification

14. KEY WORDS	LINK A		LINK B		LINK C	
	ROLE	WT	ROLE	WT	ROLE	WT
Electrofluidmechanics						
Corona Discharge						
Ion Flow						
Friction Factor						
Electric Field						
Ionization						
Electrostatic						
Induced Electric Field in Channel Flow						
Electroviscosity						

INSTRUCTIONS

1. **ORIGINATING ACTIVITY:** Enter the name and address of the contractor, subcontractor, grantee, Department of Defense activity or other organization *(corporate author)* issuing the report.

2a. **REPORT SECURITY CLASSIFICATION:** Enter the overall security classification of the report. Indicate whether "Restricted Data" is included. Marking is to be in accordance with appropriate security regulations.

2b. **GROUP:** Automatic downgrading is specified in DoD Directive 5200.10 and Armed Forces Industrial Manual. Enter the group number. Also, when applicable, show that optional markings have been used for Group 3 and Group 4 as authorized.

3. **REPORT TITLE:** Enter the complete report title in all capital letters. Titles in all cases should be unclassified. If a meaningful title cannot be selected without classification, show title classification in all capitals in parenthesis immediately following the title.

4. **DESCRIPTIVE NOTES:** If appropriate, enter the type of report, e.g., interim, progress, summary, annual, or final. Give the inclusive dates when a specific reporting period is covered.

5. **AUTHOR(S):** Enter the name(s) of author(s) as shown on or in the report. Enter last name, first name, middle initial. If military, show rank and branch of service. The name of the principal author is an absolute minimum requirement.

6. **REPORT DATE:** Enter the date of the report as day, month, year; or month, year. If more than one date appears on the report, use date of publication.

7a. **TOTAL NUMBER OF PAGES:** The total page count should follow normal pagination procedures, i.e., enter the number of pages containing information.

7b. **NUMBER OF REFERENCES:** Enter the total number of references cited in the report.

8a. **CONTRACT OR GRANT NUMBER:** If appropriate, enter the applicable number of the contract or grant under which the report was written.

8b, 8c, & 8d. **PROJECT NUMBER:** Enter the appropriate military department identification, such as project number, subproject number, system numbers, task number, etc.

9a. **ORIGINATOR'S REPORT NUMBER(S):** Enter the official report number by which the document will be identified and controlled by the originating activity. This number must be unique to this report.

9b. **OTHER REPORT NUMBER(S):** If the report has been assigned any other report numbers *(either by the originator or by the sponsor)*, also enter this number(s).

10. **AVAILABILITY/LIMITATION NOTICES:** Enter any limitations on further dissemination of the report, other than those imposed by security classification, using standard statements such as:

(1) "Qualified requesters may obtain copies of this report from DDC."

(2) "Foreign announcement and dissemination of this report by DDC is not authorized."

(3) "U. S. Government agencies may obtain copies of this report directly from DDC. Other qualified DDC users shall request through _____."

(4) "U. S. military agencies may obtain copies of this report directly from DDC. Other qualified users shall request through _____."

(5) "All distribution of this report is controlled. Qualified DDC users shall request through _____."

If the report has been furnished to the Office of Technical Services, Department of Commerce, for sale to the public, indicate this fact and enter the price, if known.

11. **SUPPLEMENTARY NOTES:** Use for additional explanatory notes.

12. **SPONSORING MILITARY ACTIVITY:** Enter the name of the departmental project office or laboratory sponsoring *(paying for)* the research and development. Include address.

13. **ABSTRACT:** Enter an abstract giving a brief and factual summary of the document indicative of the report, even though it may also appear elsewhere in the body of the technical report. If additional space is required, a continuation sheet shall be attached.

It is highly desirable that the abstract of classified reports be unclassified. Each paragraph of the abstract shall end with an indication of the military security classification of the information in the paragraph, represented as *(TS), (S), (C), or (U)*.

There is no limitation on the length of the abstract. However, the suggested length is from 150 to 225 words.

14. **KEY WORDS:** Key words are technically meaningful terms or short phrases that characterize a report and may be used as index entries for cataloging the report. Key words must be selected so that no security classification is required. Identifiers, such as equipment model designation, trade name, military project code name, geographic location, may be used as key words but will be followed by an indication of technical context. The assignment of links, rules, and weights is optional

GPO 886-551

4942.2-E

TECHNICAL REPORT # 2 Contract DA-31-124-ARO-D-246 December 16, 1966

ERRATA - May 1967

The following corrections are applicable to Technical Report # 2 (unclassified) "The Effect of Transverse Ion Current on the Flow of Air in a Flat Duct," by E. Pejack and H. Velkoff.

Page 3 Item I - Change last term of Eq. (2) to $\rho_c E_y$
Item II - Fifth line after Eq. (8) change $\partial_\rho \partial_z$ to ∂_p/∂_z

Page 4 Item I - Change E_y to E_y^2
Item II - Change J_{yy} to $J_y y$

Page 6 Item I - Change exponent on bracket to $+\frac{1}{2}$
Item II - Line 2 after Eq. (25) change Eq. (19) to Eq. (20)
Item III - Change right side of Eq. (26) to read $\left(\frac{2J_y \epsilon}{HK}\right)^{1/2}$
Item IV - Equation following Eq. (27) right side should read $\left[\frac{2J_y \epsilon}{HK}\right]^{1/2} \frac{H^2}{\mu K}$

Item V - In Eq. (28) change material inside bracket to read $\left[1 - \frac{\cosh N_{\rho c}^{1/2}\, \eta}{\cosh N_{\rho c}^{1/2}}\right]$

Page 7 Item I - Line following Eq. (32) change to read $\partial p^*/\partial \xi$
Item II - Equation (33) -- close parentheses after $\frac{N_{\rho c}}{3}$
Item III - Change numerator of right side of Eq. (30) to read $2N_{\rho c}^{3/2}$

Page 8 Item I - Eq. (37) Change $\partial p/\partial \xi$ to $\partial p^*/\partial \xi$

Page 10 Item I - Eq. (38) Change $\partial p/\partial \xi$ to $\partial p^*/\partial \xi$
Item II - Eq. (43) Change $\partial p/\partial \xi$ to $\partial p^*/\partial \xi$

Page 11 Item I - First item in first column of table should read $\left[\frac{2J_y \epsilon}{KH}\right]^{1/2}$

Page 12 Item I - Second paragraph change $f = \partial p/\partial \xi$ to $f = -\partial p^*/\partial \xi$
Item II - Eq. (45) put exponent -1 on second set of brackets

Page 13 Item I - Ordinate should read $\eta = y/H$

Page 14 Item I - Change $\frac{\partial p}{\partial \xi}$ to $\frac{\partial p^*}{\partial \xi}$

Page 15 Item I - Following Eq. (49) change J_y to $2J_y$

ERRATA for TECHNICAL REPORT # 2 December 16, 1966 Contract DA-31-124-ARO-D-246

Page 16 Item I - Fourth Paragraph, line 2, delete t after 5

Page 28 Item I - Delete H in equation at top of page

Page 30 Item I - Ordinate should read p*

Page 38 Item I - Third paragraph, last line, should read $\partial p/\partial y$

Page 45 Item I - Label symbols ○ $N_{pc} = 0$
△ $N_{pc} = 7.08$
□ $N_{pc} = 3.52$

Item II - Write "Location A" on graph

Page 46 Item I - Change $N_{RE} = 530$ to read $N_{RE} = 540$

Page 66 Item I - Change Eq. (77) -- $\partial p/\partial t$ should read $\partial p/\partial z$
Item II - Change Eq (78) -- N_{α} should read N
Item III - In equation following Eq. (78) change E to ϵ and W_m^2 to w_m^2

Page 70 Item I - Label ○ D = .031 inch
△ D = .0 inch